

**POLITECNICO DI TORINO**

Master's degree course in Mechatronic Engineering

# Condition Monitoring of Hydraulic pumps for Fluid Power Applications



**Advisor:**

Prof. Luigi Mazza

Prof. Andrea Vacca

**Candidate:**

Luca Vaccino s266561

Academic Year 2020/2021



*To my family and my friends*

# Acknowledgements

All this amazing experience would have not been possible without the professors Luigi Mazza and Andrea Vacca, who always helped and advised me in the best possible way.

A huge thanks go to all the Maha people, who helped me to reach my goals and supported me every day.

Thanks to Federico, Mateus, Riccardo, Sangbeom, Shanmukh, Swarnava and all the other guys for all the help received this year far from home. Thanks, Dave for all the practical skills that you taught me.

Thanks to my mentor Annalisa for her availability, patience, and support.

Thanks to Patrick, Hailey, Matt, Whitney and Angela for showing me all the beauties of this amazing country and make me feel at home.

Thanks to my roommate Ali Kumael who always motivated me to do better during the last months.

Finally, I want to acknowledge all my Italian friends to have been so near despite the geographical distance.

# Abstract

Nowadays, condition monitoring is becoming crucial to increase productivity and reduce Maintenance and asset downtime. However, one of the most significant limits is that too many data are required obtain a robust and reliable algorithm.

Getting those data from the experiment is costly both in terms of time and money. Furthermore, damaging components to generate faulty data is not always possible. In this thesis, a lumped parameter model will be used to generate different fault levels in an axial piston pump. To validate the lumped parameter model, a test with both a healthy pump and an Extremely damaged valve plate pump will be run.

Experimental results will be commented and analyzed.

Plus, feature selection and feature reduction will be performed in order to make the condition monitoring model as fast and reliable as possible.

Furthermore, different models will be presented and final results will be shown.

Finally, future solutions and improvement will be explained.

# Summary

<b>1</b>	<b>INTRODUCTION</b>	<b>14</b>
1.1	Motivations	14
1.2	Research goals	14
1.3	Organization	15
<b>2</b>	<b>STATE OF THE ART</b>	<b>16</b>
2.1	Spectral analysis of vibration	16
2.2	Machine Learning	16
<b>3</b>	<b>REFERENCE PUMP</b>	<b>18</b>
3.1	Introduction	18
3.2	Working principle	19
3.3	Main components and common faults	21
3.3.1	<i>Slipper</i>	22
3.3.2	<i>Piston</i>	22
3.3.3	<i>Slipper retainer</i>	23
3.3.4	<i>Cylinder block</i>	23
3.3.5	<i>Swashplate</i>	23
3.3.6	<i>Valve plate</i>	24
<b>4</b>	<b>PUMP MODEL</b>	<b>27</b>
4.1	Block Diagram	27
4.2	Drain flow estimation	30
4.3	Fault models	32
4.3.1	<i>Cylinder damage</i>	32
4.3.2	<i>Slipper damage</i>	33
4.3.3	<i>Valve plate Extreme Damage</i>	34
<b>5</b>	<b>EXPERIMENTAL TEST</b>	<b>36</b>
5.1	Testing procedure	36
5.2	Experimental results	40
5.3	ISO 46 vs ISO 32 comparison	41
5.4	Pressure ripple comparison	44
<b>6</b>	<b>MODEL RESULTS AND VALIDATION</b>	<b>46</b>
6.1	Drain flow	46

6.2	Outlet flow .....	48
6.3	Drain pressure.....	49
6.4	Extreme damage model validation .....	49
6.5	Drain pressure estimation .....	54
7	CONDITION MONITORING MODEL.....	55
7.1	Machine learning introduction .....	56
7.2	Supervised learning models .....	57
7.2.1	<i>Support vector machine (SVM)</i> .....	57
7.2.2	<i>K-nearest neighbor</i> .....	59
7.2.3	<i>Decision tree</i> .....	61
8	CONDITION MONITORING RESULTS .....	63
8.1	Test 1: Healthy / Unhealthy Detection .....	63
8.1.1	<i>Steady state values only</i> .....	63
8.1.2	<i>Pressure ripple variance only</i> .....	65
8.1.3	<i>Steady state values and pressure ripple variance</i> .....	66
8.2	Test 2: Different Damages, No Combination.....	68
8.3	Test 3: Multiple Faults .....	70
9	CONCLUSIONS AND FUTURE WORK .....	73
	Appendix 1: AVAS tool .....	74
	Appendix 2: sensors calibration .....	75
	Appendix 3: Fft And Nyquist's Theorem .....	77
10	Bibliography.....	79

# List of figures

Figure 1: MLP structure .....	17
Figure 2: different types of pumps .....	18
Figure 3: reference unit .....	19
Figure 4: pump main elements .....	20
Figure 5: pump section and main geometrical parameters .....	20
Figure 6: oil contamination damage .....	22
Figure 7: lack of lubrication damage.....	22
Figure 8: healthy slipper .....	22
Figure 9: cylinder damage (lack of lubrication) .....	22
Figure 10: cylinder damage (oil contamination).....	22
Figure 11: slipper retainer damage.....	23
Figure 12: cylinder block damage (lack of lubrication).....	23
Figure 13: swashplate damage (oil contaminants).....	24
Figure 14: extremely damage valveplate.....	24
Figure 15: relief groove detail (Yamauchi and Yamamoto,1976).....	25
Figure 16: Valve plate main geometrical parameters .....	25
Figure 17: Healthy model block diagram.....	27
Figure 18: opening area for high pressure and low-pressure port.....	28
Figure 19: cross porting area between high pressure and low pressure port .....	29
Figure 20: section view of an axial piston pump .....	29
Figure 21: valveplate drawing.....	29
Figure 22: main leakage interfaces in axial piston pump .....	31
Figure 23: piston damaged by oil contaminants .....	32
Figure 24: lack of lubrication damaged slipper.....	33
Figure 25: slipper CAD section detail .....	34
Figure 26: Extremely damaged valve plate.....	34
Figure 27: orifice equation.....	34
Figure 28: comparison between healthy valve plate and extremely damaged valve plate....	35
Figure 29: valve plate fault model implementation .....	35
Figure 30: testing procedure flowchart .....	37
Figure 31: steady state testrig ISO schematic.....	38
Figure 32: acquisition system wiring schematic .....	39
Figure 33: example of measured output pressure .....	40
Figure 34: example of measured outlet flow .....	40
Figure 35: orifice flow coefficient vs square root of Reynolds number .....	41
Figure 36: drain flow comparison for different oil types.....	42
Figure 37: Output flow comparison for different oil types .....	43
Figure 38: pressure ripple magnitude comparison.....	44
Figure 39: pressure ripple fft comparison .....	44
Figure 40: drain flow error, 1500 rpm .....	46
Figure 41: drain flow vs outlet pressure, 1500 rpm .....	46
Figure 42: drain flow error, 2000 rpm .....	47

Figure 43: drain flow vs outlet pressure, 2000 rpm .....	47
Figure 44: drain flow error, 1800 rpm .....	47
Figure 45: drain flow vs outlet pressure, 1800 rpm .....	47
Figure 47: outlet flow vs outlet pressure, 1500 rpm .....	48
Figure 46: output flow error, 1500 rpm.....	48
Figure 48: outlet flow error, 1800 rpm .....	48
Figure 49: outlet flow vs outlet pressure, 1800 rpm .....	48
Figure 50: output flow model error, 2000 rpm .....	49
Figure 51: output flow vs output pressure, 2000 rpm .....	49
Figure 52: extremely damaged valveplate CAD.....	50
Figure 53: extremely damaged valveplate .....	50
Figure 54: comparison between healthy and unhealthy groove area .....	50
Figure 55: leakage flow error .....	51
Figure 56: Comparison between Reynolds number and flow coefficient for exp. data .....	51
Figure 57: density vs temperature plot .....	52
Figure 58: viscosity vs temperature plot .....	52
Figure 59: leakage flow error – validation at 1800 rpm .....	53
Figure 60: leakage flow model error .....	53
Figure 61: drain pressure vs drain flow, healthy and ED data.....	54
Figure 62: line model error, healthy and ED data.....	54
Figure 63: general condition monitoring model workflow.....	55
Figure 64: alternative condition monitoring model workflow .....	55
Figure 65: difference between underfitting, appropriate capacity and overfitting.....	57
Figure 66: one to rest SVM approach .....	58
Figure 67: one to one SVM approach .....	58
Figure 68: classification problem in xy plane.....	58
Figure 69: classification problem in xz plane.....	58
Figure 70: kernel method representation .....	59
Figure 71; k-nn problem representation .....	59
Figure 72: Manhattan vs Euclidean distance .....	60
Figure 73: decision tree example.....	61
Figure 74: confusion matrix .....	63
Figure 75: confusion matrix for test 1a.....	64
Figure 76: speed vs estimated drain flow .....	65
Figure 77: confusion matrix for test 1b .....	66
Figure 78: confusion matrix for test 1c.....	67
Figure 79: Confusion matrix test 2.....	68
Figure 80: class 5 real fault .....	69
Figure 81: class 6 real fault .....	69
Figure 82: class 1 real fault .....	69
Figure 83: class 0 real fault .....	69
Figure 84: confusion matrix test 3 .....	70
Figure 85: class 2 real fault .....	71
Figure 86: class 1 real fault .....	71
Figure 87: class 0 real fault .....	71
Figure 88: class 5 real fault .....	71
Figure 89: class 4 real fault .....	71

Figure 90: class 3 real fault .....	71
Figure 91: class 7 real fault .....	71
Figure 92: class 6 real fault .....	71
Figure 93: example of fluid volume used for minimum area computation .....	74
Figure 94: AVAS tool workflow .....	74
Figure 95: example of area file .....	75
Figure 96: example of hand pump used to test pressure sensors.....	76
Figure 97: pressure vs voltage plot.....	76
Figure 98: example of aliasing effect.....	78

# List of equations

Eq. 1: piston stroke .....	21
Eq. 2: piston maximum stroke .....	21
Eq. 3: piston speed.....	21
Eq. 4: piston acceleration.....	21
Eq. 5: orifice equation .....	28
Eq. 6: discharge chamber volume.....	29
Eq. 7: flow between stationary and moving plate.....	30
Eq. 8: steady flow in annulus between circular shaft and cylinder .....	30
Eq. 9: healthy flow drain estimation.....	31
Eq. 10: drain flow estimation cost function.....	31
Eq. 11: general orifice equation.....	32
Eq. 12: pressure constraints .....	32
Eq. 13: simplified orifice equation .....	32
Eq. 14: cylinder damage model .....	33
Eq. 15: damaged slipper drain flow estimation.....	33
Eq. 16: orifice equation.....	41
Eq. 17: Reynolds number equation .....	41
Eq. 18: relation between output pump flow and Reynolds number.....	42
Eq. 19: output pump flow ration compared to oil density ratio .....	42
Eq. 20: drain pressure esrimation cost function.....	49
Eq. 21: Reynolds equation .....	51
Eq. 22: Reynolds number and orifice Equation .....	53
Eq. 23: Reynolds number vs orifice flow coefficient .....	53
Eq. 24: critical ratio .....	53
Eq. 25: Entropy equation .....	61
Eq. 26: Information gain .....	61
Eq. 27: Gini impurity index.....	62
Eq. 28: probability distribution .....	62
Eq. 29: Gini index: alternative formula .....	62
Eq. 30: variance.....	65
Eq. 31: discrete Fourier transform.....	77
Eq. 32: DFT decomposition .....	77
Eq. 33: DFT decomposition - part 2 .....	77

# Symbols list

Symbol	Description	Units
$a_k$	piston acceleration	[m/s <sup>2</sup> ]
$\beta$	swashplate angle	[deg]
$f_s$	sampling frequency	[Hz]
$p_d$	drain pressure	[bar]
$p_{in}$	inlet pressure	[bar]
$p_{out}$	output pressure	[bar]
$p_c$	control pressure	[bar]
$Q_A$	outlet flow	[l/min]
$Q_C$	control flow	[l/min]
$Q_D$	drain flow	[l/min]
M	torque	[Nm]
n	speed	[m/s]
$s_k$	cylinder stroke	[mm]
$t$	time	[s]
TA	output temperature	[°C]
TD	drain temperature	[°C]
Tin	supply temperature	[°C]
TS	Sampling time	[s]
$v_k$	cylinder speed	[m/s]
$\omega$	shaft speed	[rad/min]

# Abbreviations

<b>Abbreviation</b>	<b>Description</b>
ANN	Artificial Neural Network
cyl leak	Cylinder leakage
DFT	Discrete Fourier Transform
ED	Extremely Damaged
FFT	Fast Fourier Transform
NI	National Instrument
slipper leak	slipper leakage

# 1 INTRODUCTION

## 1.1 Motivations

Axial piston pumps are widely used in aerospace, transport and heavy duty machineries. Because of harsh operating environment and wear, fault occurs very often.

If not detected in time, a single damaged component can lead to huge damages of the entire equipment and of the operators who are using the machine.

It is crucial to find a way to correctly detect in time pump faults, in the cheapest and easiest way.

Checking periodically the unit elements is not always possible in reasonable time, so other solution must be found.

Condition monitoring has become one of the best trending topics of the last few years. In fact, knowing which equipment component will broke, can greatly reduce machine stop time and spare parts cost [1]. Plus, maintenance cost can be reduced up to 50% [2]. This leads to huge money savings for industries and companies.

However, one of the major challenges is collect a large amount of data in order to train a robust condition monitoring algorithm: both healthy and unhealthy component must be tested. Damaging healthy units and running many experimental tests can be very expensive, and often it is not an available solution.

The main goal of this thesis is to use a machine learning classification model in order to find the least number of sensors to successfully detect different types of fault in an axial piston pump.

To train the algorithm, different faulty conditions will be generated by using a lumped parameter model of the pump. This solution is timely and computationally affordable.

The lumped model has been validated in healthy pump case and extremely damaged valveplate case.

## 1.2 Research goals

The main goal of the research is to show a procedure to use machine learning in order to design a condition monitoring models, able to detect faulty pump components with the minimum number of sensors.

The research will include:

- Pump digital twin model design
- Experimental test to validate the model in healthy condition
- Analysis and modelling of different pump faults.
- Extremely damage valve plate experimental test, to validate the model

- Data processing and filtering
- Use machine learning to find the minimum number of sensors to detect different faults
- Condition monitoring models analysis and comparison

## 1.3 Organization

The thesis will be divided in sections. The chapter 2 will show the state of the art of condition monitoring research, showing different adopted approaches and their limits and potentialities.

Chapter 3 will describe the reference pump used for the research work. The following chapter will be related to pump model and fault analysis. In chapter 5 experimental test procedure will be described. Experimental measured data will be compared with the simulated ones to validate the model.

Chapter 6 will show different condition monitoring models, and in the following chapter the model results will be presented.

Finally, in chapter 8 conclusions and future work will be shown.

# 2 STATE OF THE ART

This chapter has the goal of showing the progress and different solution adopted by other authors to face the condition monitoring topic. Every solution will be presented considering both positive aspects and possible improvements.

## 2.1 Spectral analysis of vibration

One of the oldest methods to detect fault inside a pump consist in studying the vibrations coming from the case[3]. In fact, a damaged pump component will affect the pressure ripple and the flow ripple. The pressure anomalies will be transmitted by the oil to the pump case.

Noise and vibration study started in 1965: Kane *et al.*[4] investigated the vibration produced by different faults in several hydraulic systems. In particular, they were able to show the differences in frequency domain due to air bubbles in oil by using an oscilloscope. Other sources of noise were taken into account apart from the pump: hydraulic line, mechanical vibrations and pump fluctuations can contribute to increase the pump noise.

In 1993, Wen [5] showed a method to detect slipper failures in axial piston pump, by studying the signal power spectrum measured by placing 4 accelerometers on the pump case. He showed how it is possible to understand the slipper fault level analyzing the power spectrum peak positions and magnitude.

Ten years later, Gao, Kong and Zhang [6] developed a wavelet analysis for piston pump fault diagnosis. They showed different diagnosis systems, such as diagnosis based on over-limit mean square amplitude, characteristic frequencies and time-frequency domain analysis

Recently, in 2019, Casoli and Rundo [7] presented a way to successfully detect and distinguish between different fault types (worn port plate, port plate with cavitation, worn slippers and damaged cylinder block) by dividing the frequency signal in 2 part: a constant one plus another contribute related to noise.

## 2.2 Machine Learning

Machine learning is a relatively recent method, based on letting the solver find a correlation between the input data. It is advantageous because a fully precise and complete knowledge of the studied system is not required.

In 1997 Watton and Pham[8] used multilayer perceptron (MLP) type neural networks to predict variation in pump outlet flow due to different types of damages. Finally they showed that this method would be able to detect correctly two different cylinder leakages.

MLP is a particular type of neural network in which there are always one input layer, one hidden layer and one output layer. A multilayer perceptron can be represented as in figure 1.

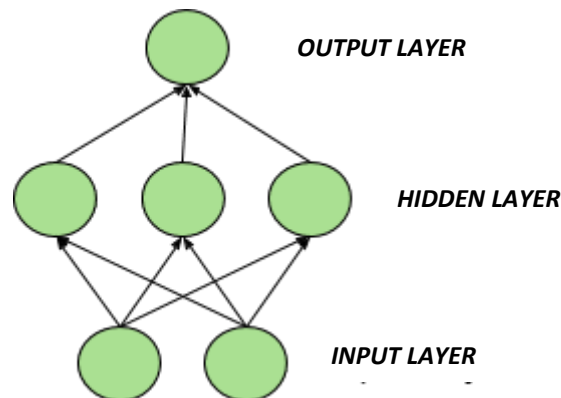


Figure 1: MLP structure

In this figure, the circles represent neurons. A row of neurons is called layer. Each neuron receives an input, which will pass through a transfer function, which is a function able to give different weights to different inputs.

In 2013, Kivela and Mattila[9] introduced a multivariable histogram method for condition monitoring. This method is based on finding relations between different variables by using multi-dimension histograms. After having collected data for different faulty conditions, the MVH model is trained and validated.

To detect faults, the measured data are compared with the model. In this approach, the model is used as “map”, and a lot of experimental data are required for having good accuracy.

A convolutional neural network approach to detect faulty pump elements have been shown by Yan et al. in 2016[10]

This approach is more accurate with respect to multi-layer perceptron because it is able to detect spatial and temporal relationship between data, by using different filters[11]. Those filters have the function to divide the dataset into smaller datasets, in order to find feature correlations with a relatively low computational effort

Recently, in 2018, Lan, Hu et al [12] presented a method to diagnose slipper abrasion of axial piston pump by using extreme learning machine (ELM). This kind of machine learning algorithm is based on feedforward neural networks. This solution is faster with respect to standard neural networks[13]. This solution, however, can lead to minor accuracy[14]

# 3 REFERENCE PUMP

## 3.1 Introduction

In general, pumps are units able to convert mechanical energy (provided by a rotating motor) into hydraulic energy (transmitted to the actuators by a hydraulic fluid, in general oil). They can be divided into different categories. The figure 2 shows different types of pumps[15].

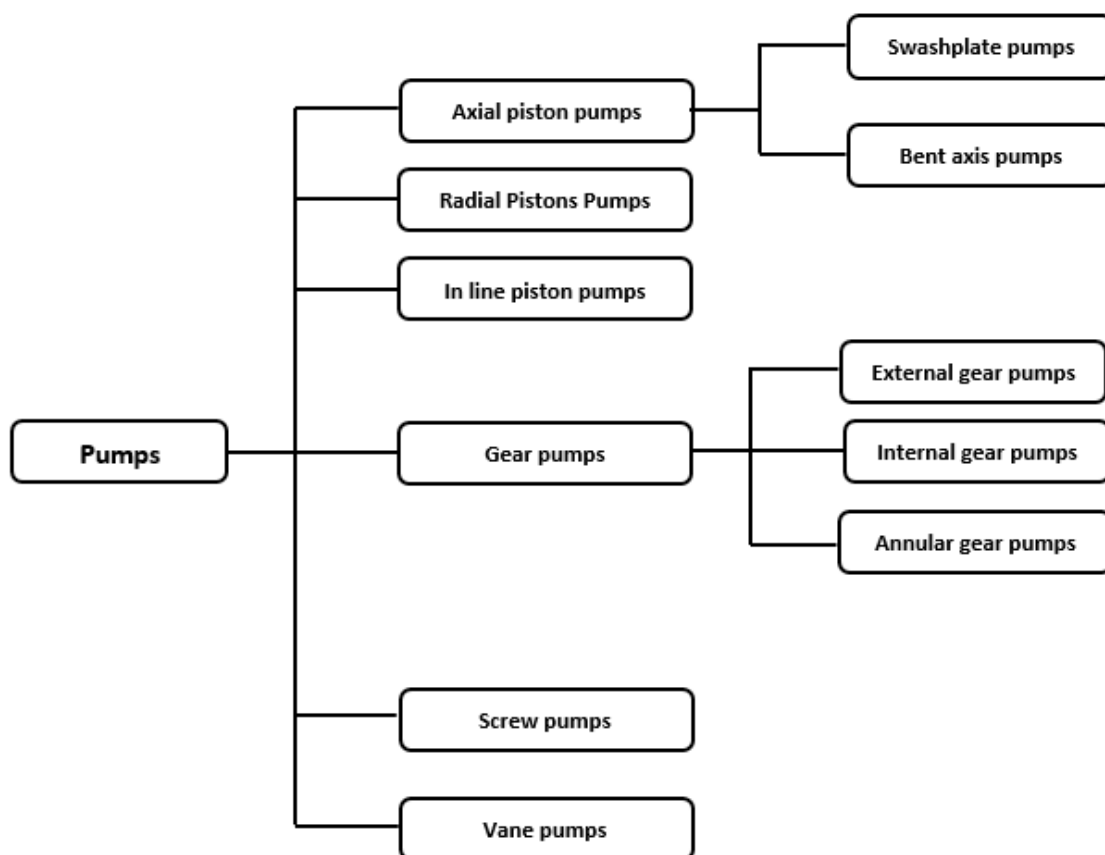


Figure 2: different types of pumps

The reference unit chosen for this research work is a P18cc axial piston pump. The main reason of this choice is the availability of many units and the large amount of research done by previous researchers at Maha. The testing procedure and the hydraulic circuit didn't require any relevant changes with respect to the one used in N. Keller research[16]. Finally, this unit is also used on a 5T excavator for the main actuators. That means that in future the developed condition monitoring algorithm could be tested on a real heavy duty machine.

The unit used in this thesis is shown in figure 3, taken from Parker catalog.



Figure 3: reference unit

## 3.2 Working principle

Pumps are used to convert mechanical energy, coming from an external motor, into hydraulic energy, transmitted by fluid.

The principal components of an axial piston pump are the following ones:

- Swashplate
- Pistons
- Valve plate
- Barrel
- Cylinder block
- Slippers
- Shaft

The figure 4 [17] shows those components and their positions.

The working principle of this unit can be resumed as follows. The shaft is coupled at one side to a motor, and at the other side to the cylinder block. When the shaft rotates, the cylinder block rotate at the same speed. Thus, each piston is connected either to the delivery port or to the suction port, depending on its angular position, as shown in figure iii

The stroke of each piston is controlled by the swashplate, which can be inclined from  $-19^\circ$  (negative full displacement) up to  $+19^\circ$  (positive full displacement).

The contact between swashplate and cylinders is always guaranteed by slippers: those elements are used to convert the swashplate angular motion into cylinder linear motion.

During the experimental test, the displacement has been set by a directional valve, controlled by a feedback signal. The controller type is a simple proportional control: real swashplate position is compared to the desired one. If it is smaller, more flow will be sent to the actuator. In the other case, instead, the valve will send less flow.

The P18 unit is a closed-circuit pump that can control the swashplate to the over-center position. That means that the configuration can be set to motor or pump depending on the swashplate position.

The unit will work as motor if the flow direction is entering to the unit. In the opposite case (positive displacement), the unit will work as pump. In this case, the flow direction will be exiting with respect to the unit.

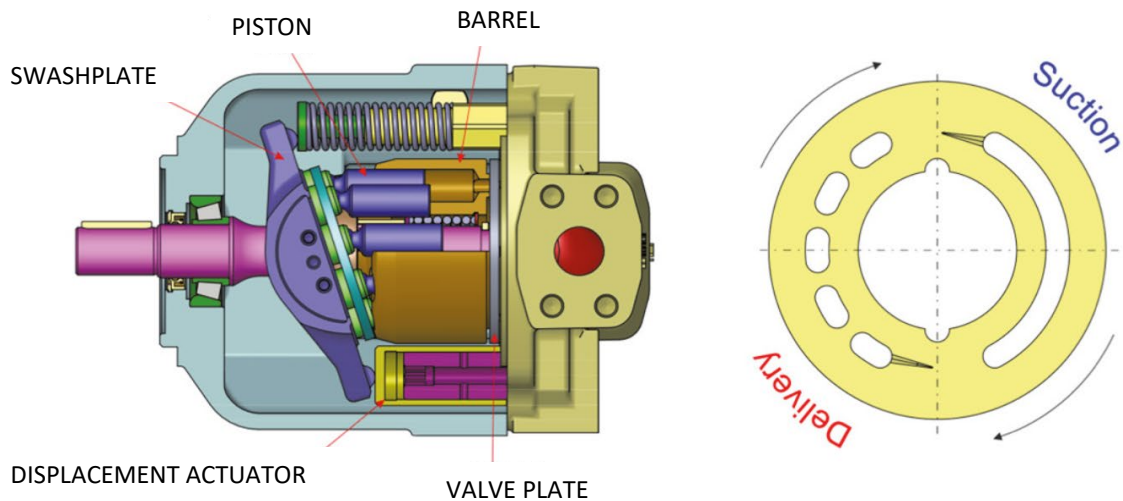


Figure 4: pump main elements

### 3.3 Pump Kinematics

To better understand the effects of each pump fault, in this paragraph the pump kinematics will be shown.

First of all, the main geometrical parameter are presented in figure 5 [18].

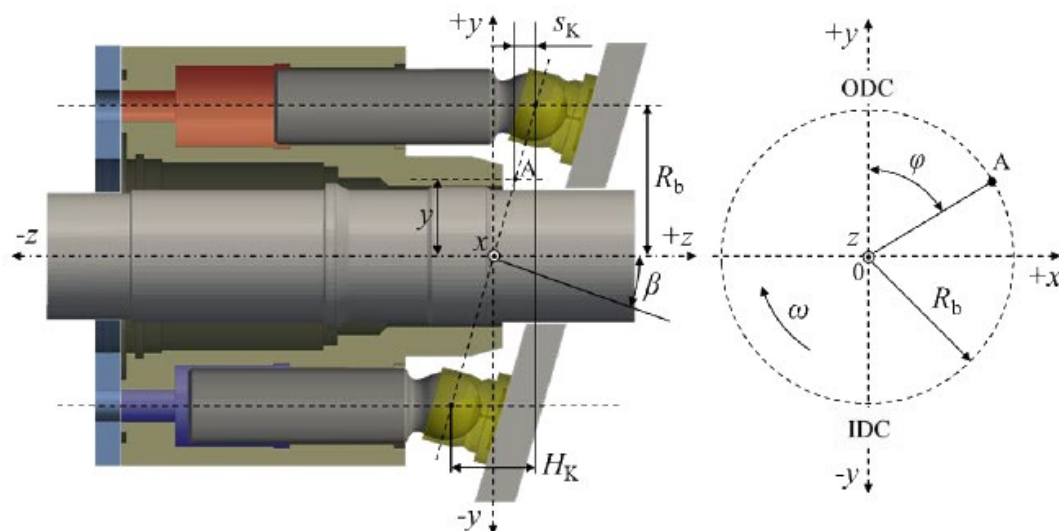


Figure 5: pump section and main geometrical parameters

The shaft is connected to a motor from one side, while from the other side is connected to the cylinder block using a spline coupling.

The cylinder block rotates together with the shaft, while the swashplate and valveplate are fixed to the pump case.

The fluid is taken from low pressure port (blue one), and it is delivered to high pressure.

Using  $\phi$  for the angular position, and  $\omega$  for the angular velocity it is possible to compute the piston stroke, piston velocity and piston acceleration.

In particular, from equation 1 it is possible to observe that the piston stroke  $s_k$  depends with the pitch radius  $R_b$ , the angular position and the swashplate angle  $\beta$ .

$$s_k = -R_b \cdot \tan\beta(1 - \cos\phi) \quad (1)$$

The maximum piston stroke can be computed as follows:

$$H_k = 2 \cdot R_b \cdot \tan\beta \quad (2)$$

From the maximum stroke, it is possible to derive the piston speed

$$v_k = \frac{ds_k}{d\phi} \cdot \omega = -\frac{1}{2} \omega \cdot H_k \cdot \sin\phi \quad (3)$$

The acceleration can be expressed by the following formula:

$$a_k = \frac{dv_k}{d\phi} \cdot \omega = -\frac{1}{2} \cdot \omega^2 \cdot H_k \cdot \cos\phi \quad (4)$$

### 3.4 Main components and common faults

Since axial piston pumps are widely used in harsh environments, all the components are frequently subject to faults. The main causes are reported in service manuals and are:

- Lack of lubrication
- Operating at excessive temperature
- improper fluid used
- Aerated fluid
- Abrasive contaminants
- Over speeding
- Solid contamination
- Water contamination

For each pump component, the possible damages will be shown. Most of those pictures are taken from Danfoss service manual [19].

### 3.4.1 Slipper

The piston slipper has the role of converting the swashplate angular variation into cylinder linear motion. The small hole in the center is used to deliver a small amount of oil in order to lubricate the swashplate – slipper interfaces.

The slipper element can be damaged by contaminants inside the oil or by lack of lubrication. In the first case, the slipper will be similar to figure 6. In case of lack of lubrication, instead, it will appear like in figure 7. Healthy slipper is shown in figure 8.



Figure 8: healthy



Figure 6: oil contamination damage



Figure 7: lack of lubrication damage

### 3.4.2 Piston

Each piston delivers flow to the outlet port, and pulls flow from the inlet port. The semi-spherical head is linked to the slipper. In this way the slipper will be able to rotate on this joint, being able to track the swashplate angular position. As it is possible to see in figure 9, the piston head has a small hole, used to deliver a minimum part of flow to the slipper-swashplate interface, to guarantee a constant lubrication.

One common piston damage is the discoloration due to lack of lubrication or too extreme operating temperature



Figure 9: cylinder damage (lack of lubrication)

Another fault that often occurs is the scratch due to fluid contamination, as shown in figure 10



Figure 10: cylinder damage (oil contamination)

### 3.4.3 Slipper retainer

This element is used to keep the piston slippers parallel between each others. It is very sensitive to overspeed: as it is possible to observe in figure 11, the most fragile part is the slipper retainer edge.



Figure 11: slipper retainer damage

### 3.4.4 Cylinder block

The cylinder block is used to transmit the rotational motion from the shaft to the cylinders. When the cylinder block is rotating, the cylinders enter in contact with the high pressure port and the low pressure port, depending on their own angular position. The main fault that occurs is the wear of cylinder block - slipper interface and cylinder block - valve plate interface (figure 12)



Figure 12: cylinder block damage (lack of lubrication)

### 3.4.5 Swashplate

To change the pump displacement, the inclination of this element is changed, by controlling 2 control cylinders, which act on 2 hinges (figure 13)

The swashplate is very sensitive to the presence of contaminants in fluid. If the swashplate is damaged, probably the slippers will be damaged too, because they slide on the swashplate when the cylinder block rotates.

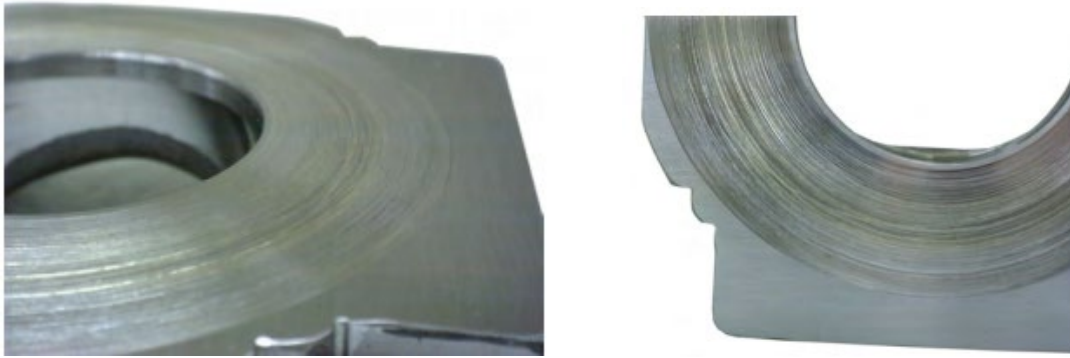


Figure 13: swashplate damage (oil contaminants)

### 3.4.6 Valve plate

This element is crucial for noise reduction and pressure ripple mitigation. In particular, the groove in correspondence of the high pressure and low pressure port starting point are crucial to guarantee a smooth transition between the different pressure levels.

Valve plate damage can occur because of external contaminants, lack of lubrication, excessive wear or too high temperature.

For research purposes, an extreme damage due to contamination has been simulated.

This is visible in picture iii. This kind of damage has been created by artificially damaging the valve plate simulating a 0.35 mm depth scratch (figure 14)

The effect of this scratch is expected to not only increase the pressure ripple, but also deliver a certain amount of flow to case. In fact, in correspondence of the finishing part of the scratch, the valve plate will not be fully sealed toward the cylinder block.

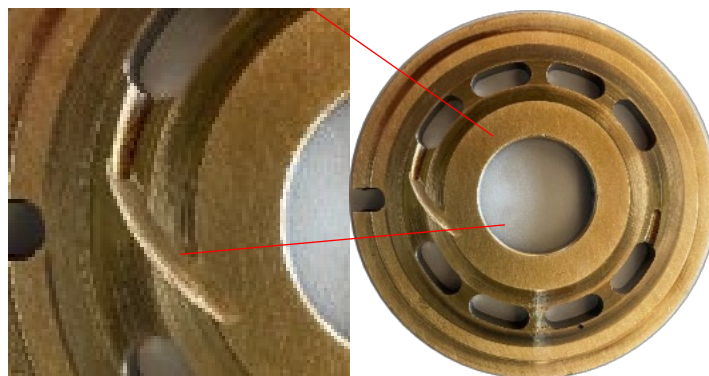


Figure 14: extremely damage valveplate

From figure 12, it is possible to see 2 different grooves, in correspondence of both high pressure and low pressure port.

A more detailed view of this groove is shown in figure 15.

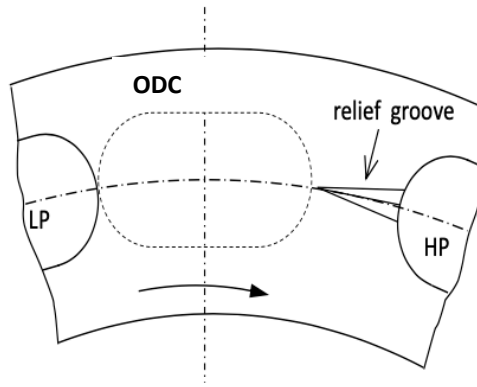


Figure 15: relief groove detail (Yamauchi and Yamamoto,1976)

From figure 16, taken from Matlab Simulink guide, a simplified version of valve plate is shown. In table 1 are shown the different opening area values depending on piston angular position.

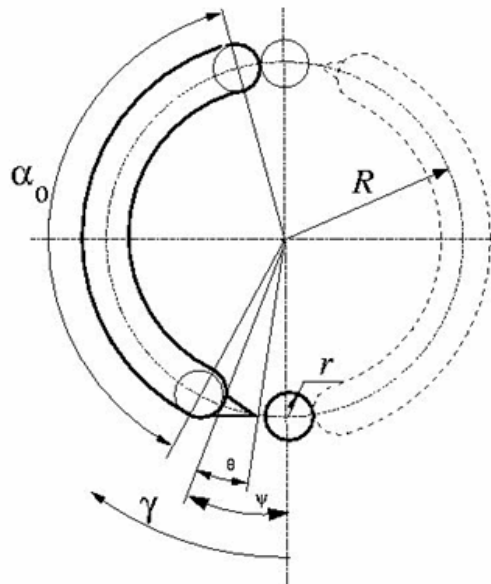


Figure 16: Valve plate main geometrical parameters

1	$\gamma_1$	$\psi - \theta - r/R$	Opening of transition slot
2	$\gamma_2$	$\psi - r/R$	Opening of major slot. Orifice still in contact with transition slot
3	$\gamma_3$	$\psi + r/R$	Major slot fully open
4	$\gamma_4$	$\psi + r/R + 0.01$	End of transition slot
5	$\gamma_5$	$\pi - 2 \cdot r/R$	End of major slot full opening
6	$\gamma_6$	$\pi$	End of major slot opening

Table 1: valve plate geometrical parameter description

The real valve plate, shown in figure 12, has 8 different slots instead of 2 major ones. However, as a first approximation they can be considered equal to 2 bigger slots, since the orifice equation is not valid anymore: the ratio between the fluid volume diameter and the kidney is quite equal to 1. Orifice equation is considered valid only when the diameter ratio is less than 0.1.

# 4 PUMP MODEL

## 4.1 Block Diagram

To model the pump, a lumped parameter approach has been used. This method has been shown that can have a quite precise accuracy with reduced computational time [17].

This kind of approach has been chosen because of the necessity to have a large amount of data in a small amount of time.

The block diagram in figure iii shows the input and output of each component.

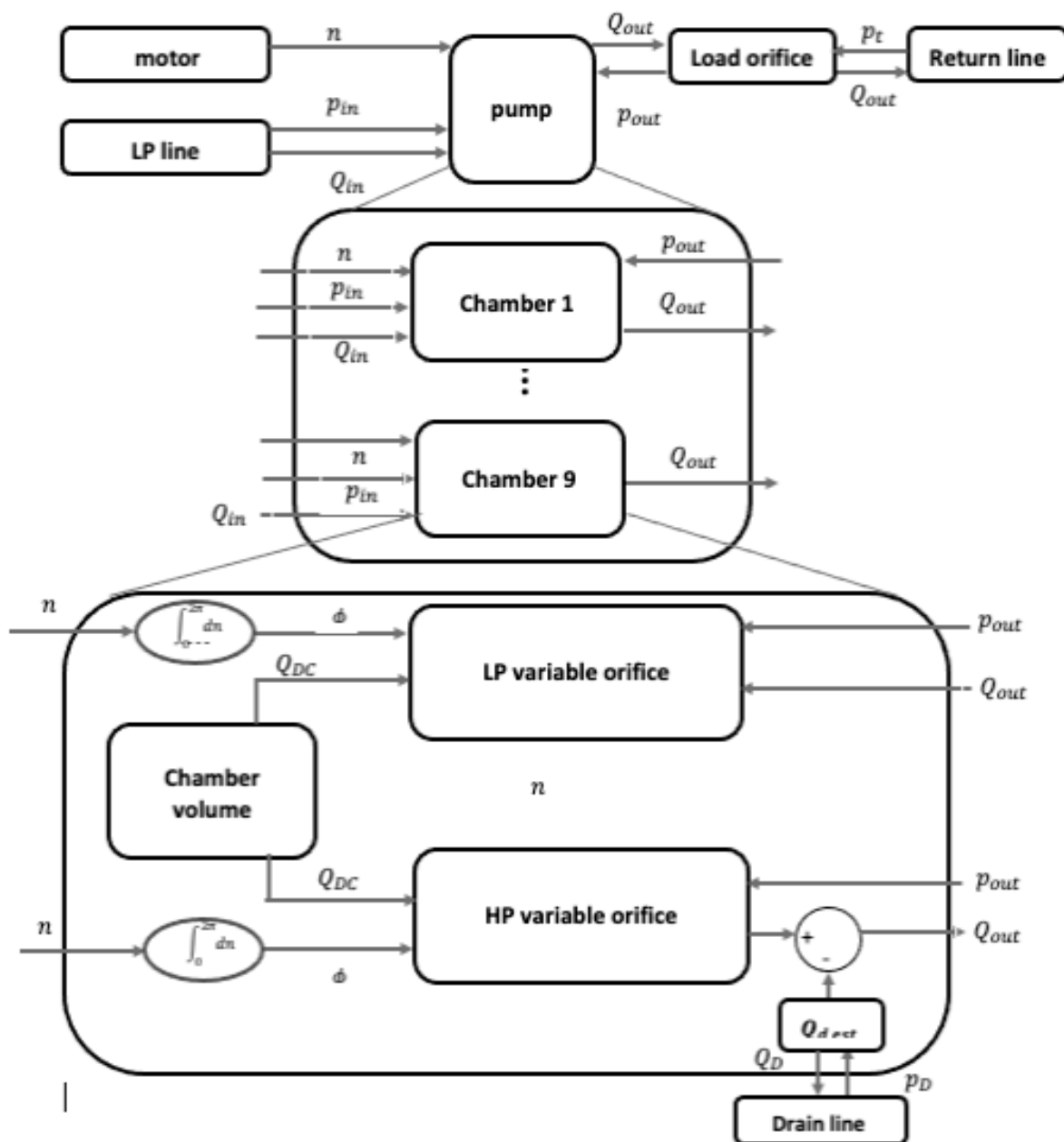


Figure 17: Healthy model block diagram

The pump block gets as input the shaft speed  $n$  and the inlet pressure  $p_{in}$ . The output pressure  $p_{out}$  is imposed: in real experimental setup it is set manually by regulating the needle valve opening.

This block, basically, can be considered as made by 9 different sub-blocks, representing the 9 pump cylinder displacement chambers. Inside those cylinders blocks, the shaft speed is converted into shaft position by integration from zero to  $2\pi$ . The shaft position is used as input to determine the correct opening area of low pressure and high-pressure variable orifices. To correlate shaft position with opening area a 1D look up table has been used.

Figure 18 shows the opening area with respect to angular position for both high pressure port and low pressure.

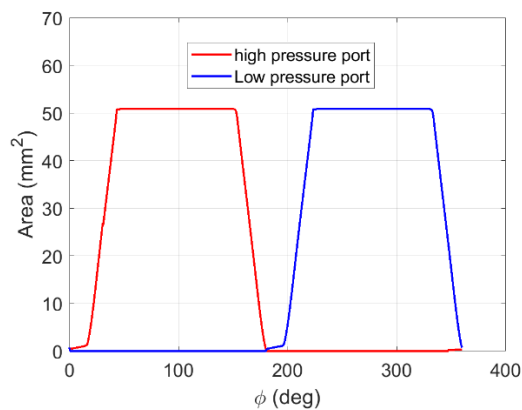


Figure 18: opening area for high pressure and low-pressure port

The relation which connect flow and pressure is shown in equation iii.

$$Q = c_f \cdot A \cdot \sqrt{\frac{2 \cdot \Delta p}{\rho}} \quad (5)$$

To get the opening area plot, AVAS (Automated Valve plate Area Search) tool has been used. Further details about this tool will be provided in appendix 1.

As it is possible to observe from figure 18, the valve plate opening area is perfectly symmetric. Special attention must be paid to the groove area, better shown in figure 19: in correspondence of 180 degrees the high pressure and low-pressure port are crossing. This phenomenon is defined cross porting, and its crucial to reduce the pressure ripple and consequently the pump noise.

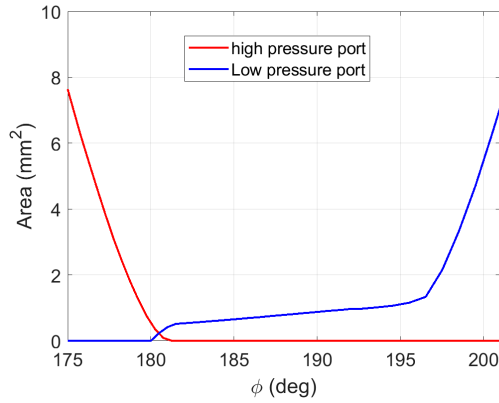


Figure 19: cross porting area between high pressure and low pressure port

The high-pressure orifice, as the name suggest, is linked to the high-pressure port as input, that is the one in which the pressure is set by acting on the needle valve.

The low-pressure port, instead, is connected to the low-pressure inlet line. In this case, the low pressure has been set by acting on the low pressure pump in the Maha Power supply room. On heavy duty machines, instead, this pressure is set by a small charge pump, which provides the desired set pressure (25 bar).

The other side of orifice blocks is linked to the displacement chamber.

This chamber has a variable volume, according to the formula 6 .

$$Ch = \frac{2\pi n}{60} \cdot R_{pitch} \cdot \tan(\beta_{max}) \cdot A_{pis} + V_{dead} \quad (6)$$

All the geometrical parameters have been taken from a CAD file or directly measured when it has been possible. In particular, the pitch radius is shown in figure iii, while the displacement is shown in figure iii.

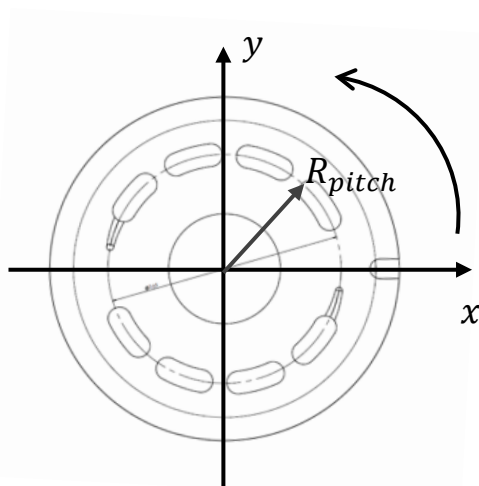


Figure 21: valveplate drawing

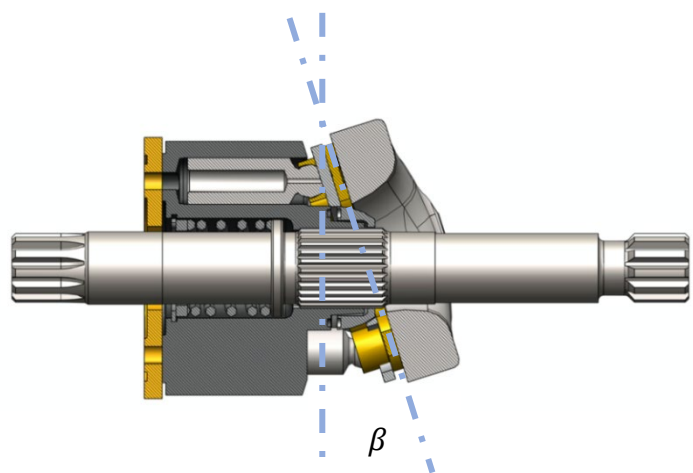


Figure 20: section view of an axial piston pump

$A_{pis}$  is the piston area, and  $V_{dead}$  is the dead volume. This is the minimum chamber volume, that is the volume of the chamber when the piston stroke is zero (minimum stroke position).

As it is possible to observe in figure iii, the flow delivered by each cylinder is sinusoidal. The phase shift is equal to  $360/9$  degrees. The over imposing of each sinusoidal gives the effective output flow. The pump has an odd number of piston to reduce the flow ripple.

The output line has been modeled as a capacitance. That could lead to some differences between the measured values and the simulated ones. In particular, the pressure ripple can present some substantial differences. In fact, the output line in the real experiment setup consist in rubber hoses, steel elbows and different fittings. Those element can be a relevant source of noise and interference with respect to the ideal output shape.

## 4.2 Drain flow estimation

To simulate the flow losses inside the pump, in healthy condition, different types of leakage has been taken into account.

As first approximation, it is possible to identify three main leakage sources:

- Piston cylinder interface
- Slipper-swashplate interface
- Valveplate-cylinder interface

Those kinds of leakages can be considered using two different formulations: flow between stationary and moving flat, parallel plates (Eq 7), and steady flow in annulus between circular shaft and cylinder (Eq iii).

$$Q = \frac{\pi D b^3 \left[ 1 + 1.5 \left( \frac{\epsilon}{b} \right)^2 \right] (P_u - P_d)}{12 \mu L} \quad (7)$$

$$Q = \left[ -\frac{b^3}{12 \mu} \frac{P_u - P_d}{L} + \frac{V_b}{2} \right] w \quad (8)$$

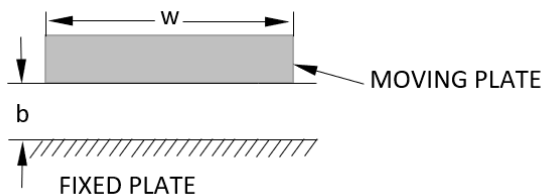


Figure 23



Figure 22

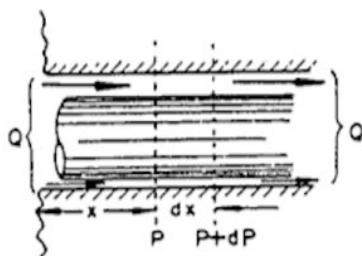


Figure 24

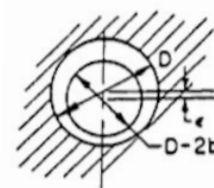


Figure 25

As first approximation, the drain flow  $Q_d$  can be assumed as series and parallel of different laminar orifices, plus an additive contribution related to velocity.

The figure iii better explains the two different approaches. The blue lines highlights the eq.7 leakages, while the green lines are related to eq 8 leakages.

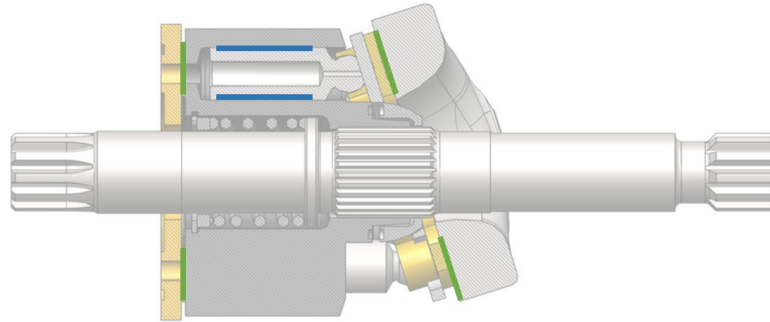


Figure 26: main leakage interfaces in axial piston pump

Since the geometrical parameters are not available only macroscopic consideration has been performed. As first approximation, the drain flow has been assumed as sum of the three previous contributes. Pressure and speed have been identified as most important factors. Thus, the drain flow it has been expressed according to formula 9

$$Q_D = x_1 \cdot p_H + x_2 \cdot p_L + x_3 \cdot n \quad (9)$$

To estimate those parameter, the measured drain flow at 1500 and 2000 rpm, with output pressure of 50,100,150,200,250 bar has been compared with the simulated one, given by formula 9.

The parameters have been determined by using a GRG nonlinear solver (Generalised Reduced Gradient).

As cost function, the minimization of Root Square Mean Error has been chosen (eq. 10)

$$C = \min \sum_{i=1}^N \frac{1}{N} \cdot \sqrt{\left( \frac{Q_{Dmeas} - Q_{Dsim}}{Q_{Dmeas}} \right)^2} \quad (10)$$

Finally, the parameters have been validated using acquired data at 1800 rpm, 50,100,150,200,250 bar as output pressure. The estimation and validation error will be shown in the results chapter.

## 4.3 Fault models

### 4.3.1 Cylinder damage

The case of a scratch produced by oil contaminant has been taken into account (figure 23). This scratch can be modeled as a fixed orifice which connects the piston chamber with the pump case.



Figure 27:piston damaged by oil contaminants

In particular, the orifice equation 13 has been implemented into the numerical model.

$$Q_{leak} = c_f \cdot A \sqrt{\frac{2 \cdot (p_{DC} - p_{case})}{\rho}} \quad (11)$$

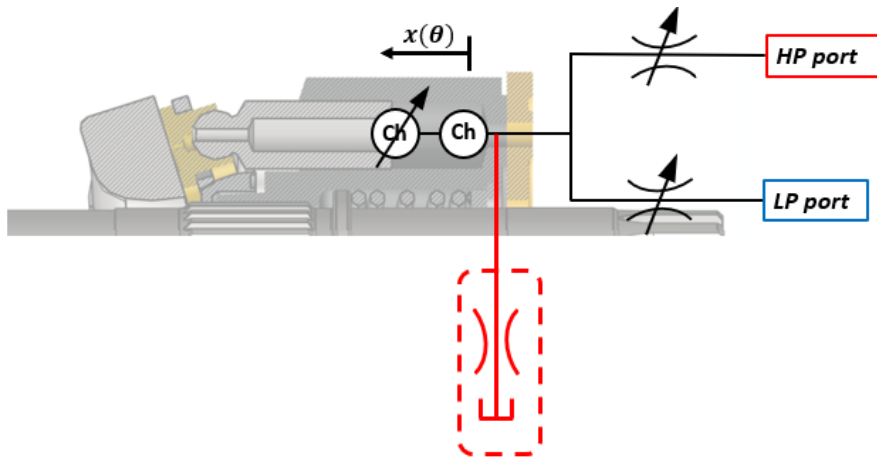
From experimental test, it has been observed that the case pressure is two orders of magnitude smaller than the displacement chamber pressure, so it is possible to assume that

$$p_{case} \ll p_{DC} = 0 \quad (12)$$

The equation 11, then, can be rewritten as equation 13

$$Q_{leak} = c_f \cdot A \sqrt{\frac{2 \cdot p_{DC}}{\rho}} \quad (13)$$

Figure iii shows the orifice implementation inside the model.



Eq. 14: cylinder damage model

#### 4.3.2 Slipper damage

A clogged slipper (figure 24) has been modeled, using overimposing effect. The procedure to estimate the healthy leakages between lubricating interfaces has been shown in chapter 5.2.



Figure 28: lack of lubrication damaged slipper

In normal operating conditions, every slipper has a little hole, used to divert some flow to the slipper-swashplate interface. This flow will guarantee a correct lubrication between the 2 interfaces.

Because of oil contamination or excessive wear, the orifice can be clogged: no more flow will pass through it.

Consequently, this flow must be subtracted to the healthy estimated one.

Formula iii has been implemented into the numerical model.

$$\left\{ \begin{array}{l} Q_{leak} = c_f \cdot A \cdot \sqrt{\frac{2 \cdot p_{DC}}{\rho}} \\ QD = x_1 \cdot (p_H) + x_2 \cdot (p_L) + x_3 \cdot n - Q_{leak} \end{array} \right. \quad (14)$$

To better understand the role of piston slipper a CAD section view is shown in figure 25. Here is possible to see that the lubricating flow is delivered to the interface between an orifice inside the piston head and another orifice inside the slipper.

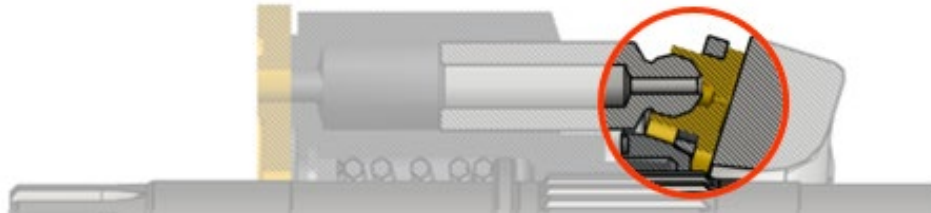


Figure 29: slipper CAD section detail

### 4.3.3 Valve plate Extreme Damage

The valve plate damage (figure 26), caused by the presence of contaminants inside oil, can be modeled considering 2 effects.



Figure 30: Extremely damaged valve plate

The first effect of the scratch is delivering a part of flow from the high pressure toward the pump case.

This effect can be modeled using the equation 15. Also in this case, the case pressure is considered neglectable with respect to the high pressure.

$$Q = c_f \cdot A \sqrt{\frac{2 \cdot p_H}{\rho}} \quad (15)$$

The second effect, that is the scratch in correspondence of the high pressure relief groove, has been modeled by changing the high pressure orifice area plot, as in figure 27.

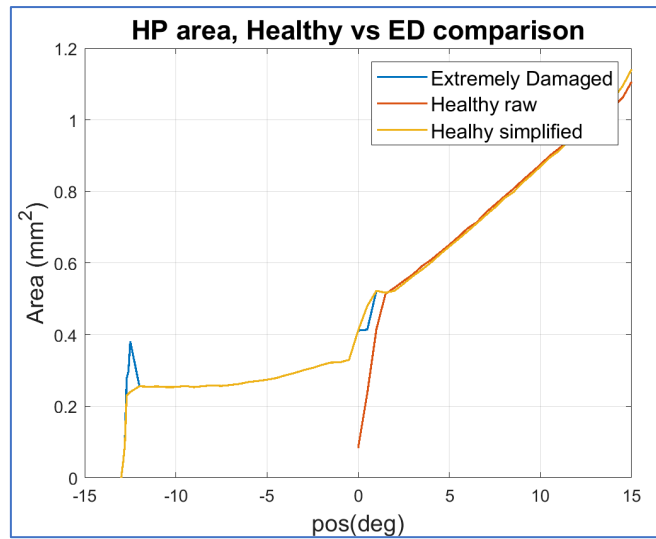


Figure 32: comparison between healthy valve plate and extremely damaged valve plate

Figure 29 shows the model implementation

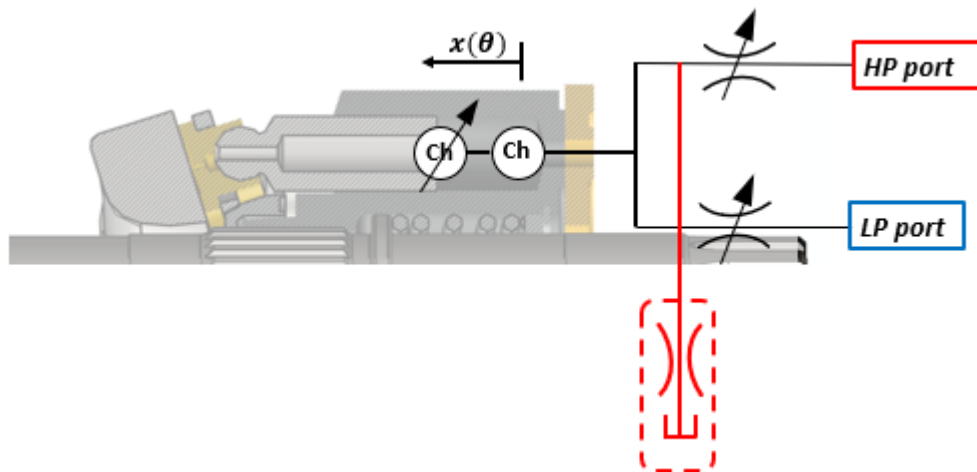


Figure 33: valve plate fault model implementation

# 5 EXPERIMENTAL TEST

For both healthy and unhealthy valveplate the same test rig has been used, with the same layout: the valveplate has been changed without removing the pump from its support. In this way shaft misalignment errors have been avoided. To disassemble the pump, the procedure present on pump service manual has been followed. Thus, the case bolt screwing torque has been checked with an adjustable wrench, set to 51 Nm (values suggested by pump manufacturer).

The ISO schematic in figure iii represent the hydraulic testrig configuration.

## 5.1 Testing procedure

Before starting the measurement part, the data acquisition system has been tested and calibrated. The calibration phase consist in finding the right scaling factors to convert the output of each sensor (that is, voltage), in physical signals (pressure, flow, temperature, pressure ripple).

To calibrate the pressure sensors, different pressure values have been set by using a hand pump. The correspondence voltage has been acquired. by plotting the pressure with respect to voltage and by finding the best fitting line, it is possible to find the correct calibration values.

Regarding to the flow meters, different flow signals have been sent to the data acquisition system box, using the VSE TB2 tool.

Then, the respective voltage has been measured. The best fitting line offset and slope values corresponds to the desired calibration parameters.

A better description of calibration phase will be provided in appendix A.

Once all the electrical connections and wiring have been checked, the testing part can be started. It can be resumed by the flow chart below.

After turning the motor on, the needle valve has been fully closed, and the pressure relief valve has been set to a value of 270 bar.

Once the pressure relief valve is properly set, the load pressure can be adjusted by acting on the needle valve.

All the measurements have been taken with an inlet temperature of 50°C, because the pump datasheet shows the values for this temperature.

The data acquisition phase started after 10 minutes that the measured inlet temperature reached the set point. This is because in this way more stable values will be measured.

In fact, during the operating conditions change, the temperature value will oscillate before reaching a stable point.

The above procedure has been repeated for all the operating conditions shown in table 2

Table 2: tested operating conditions

$n$ (rpm)	$\Delta p$ (bar)
3000	250
	200
	150
	100
	50
2000	250
	200
	150
	100
	50
1800	250
	200
	150
	100
	50
1500	250
	200
	150
	100
	50
1000	250
	200
	150
	100
	50
800	250
	200
	150
	100
	50

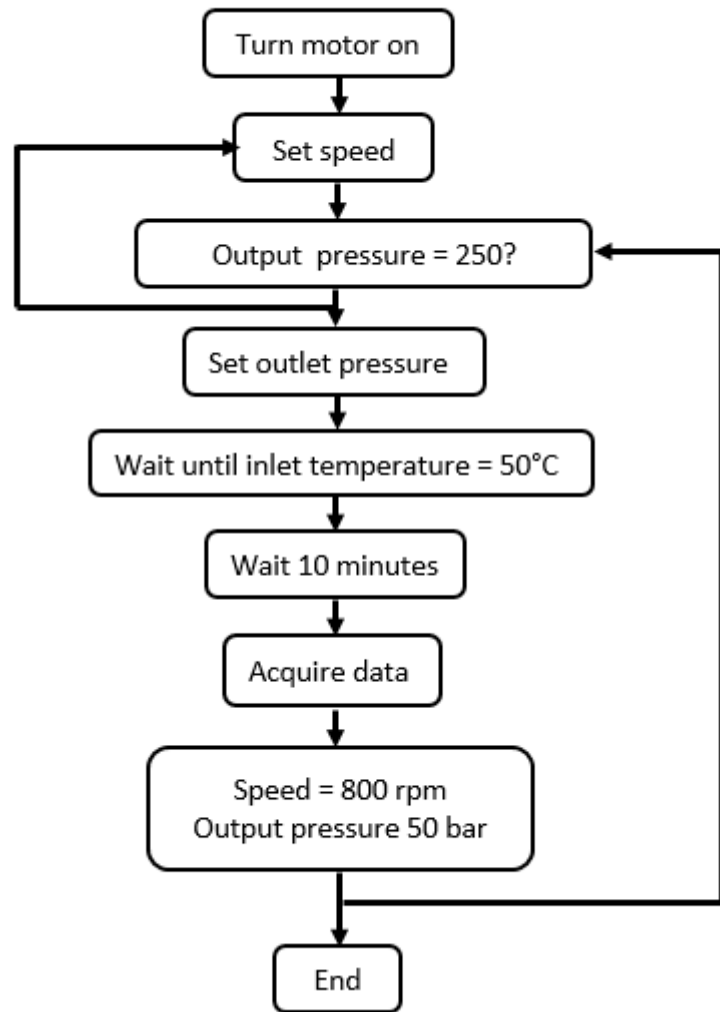


Figure 34: testing procedure flowchart

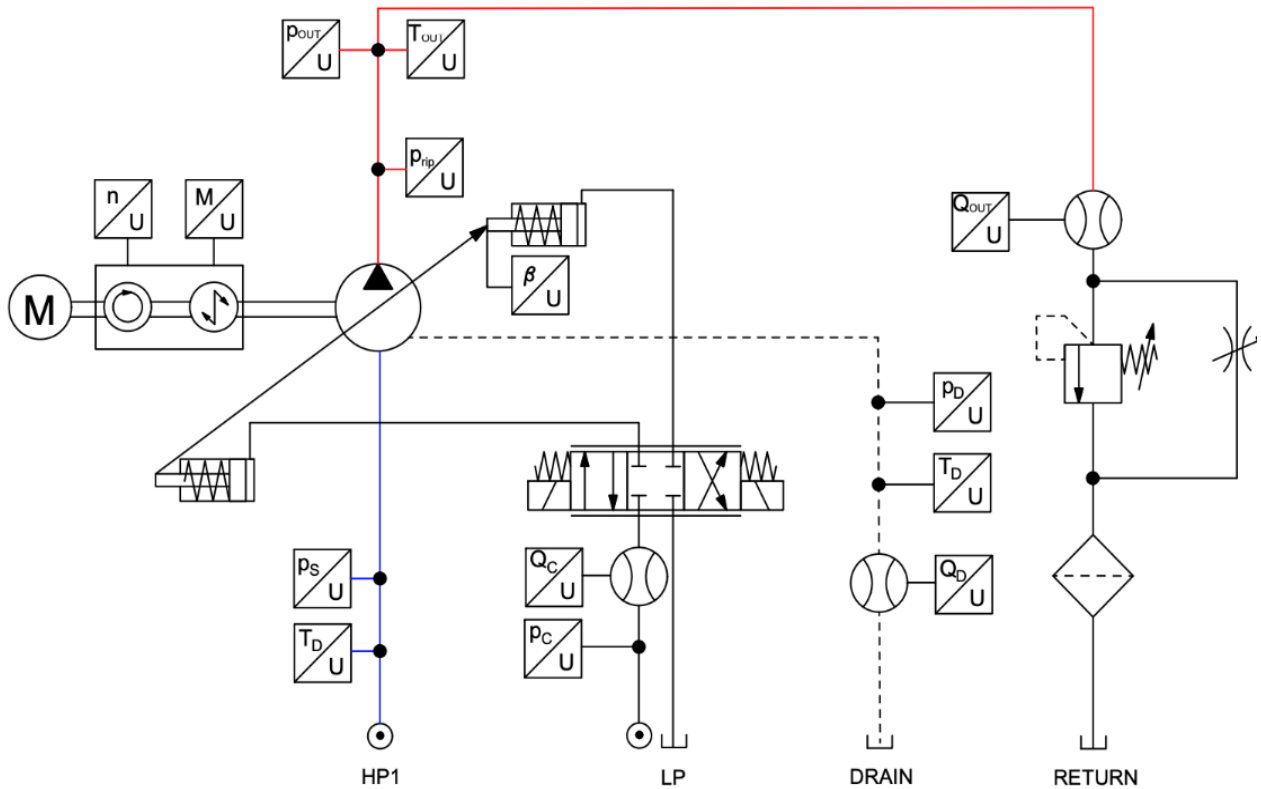


Figure 35: steady state testrig ISO schematic

Sensor	Signal	Sensor type	model	Full scale	Accuracy
1	inlet temperature	Thermocouple	Omega K	1-1250°C	0.75 % FS
2	inlet pressure	Voltage output pressure transducer	Hydac 4475-B-0150	5000 psi	0.1 % FS
3	Shaft speed	Encoder	Kistler 4503A	7000 rpm	0.1% FS
4	Torque	Torquemeter	Kistler 4503A	500Nm	0.1% FS
5	Output pressure ripple	Piezo pressure sensor	Kistler 603C	1000 bar	0.4 bar FS
6	Output pressure	Voltage output pressure transducer	Hydac 4475-B-6000	6000 psi	0.1% FS
7	Output temperature	Thermocouple	Omega K	1-1250°C	0.75 % FS
8	Output flow	Gear type flowmeter	VSI 4/16 EPO 12 T-	250 lpm	0.1% FS
9	Control pressure	Voltage output pressure transducer	Keller	30 bar	0.1% FS
10	Control flow	Gear type flowmeter	VS 0.2 EPO 12 T-	18 lpm	0.1% FS
11	Drain flow	Gear type flowmeter	VS 0.2 12V-HT/3	18 lpm	0.1% FS
12	Drain temperature	Thermocouple	Omega K	1-1250°C	0.75 % FS
13	Drain pressure	Voltage output pressure transducer	Keller Value Line	10 bar	0.1% FS
14	Swashplate position	Hall effect angular sensor	RS60	180°	1.3°

Table 3: steady state test rig sensor list

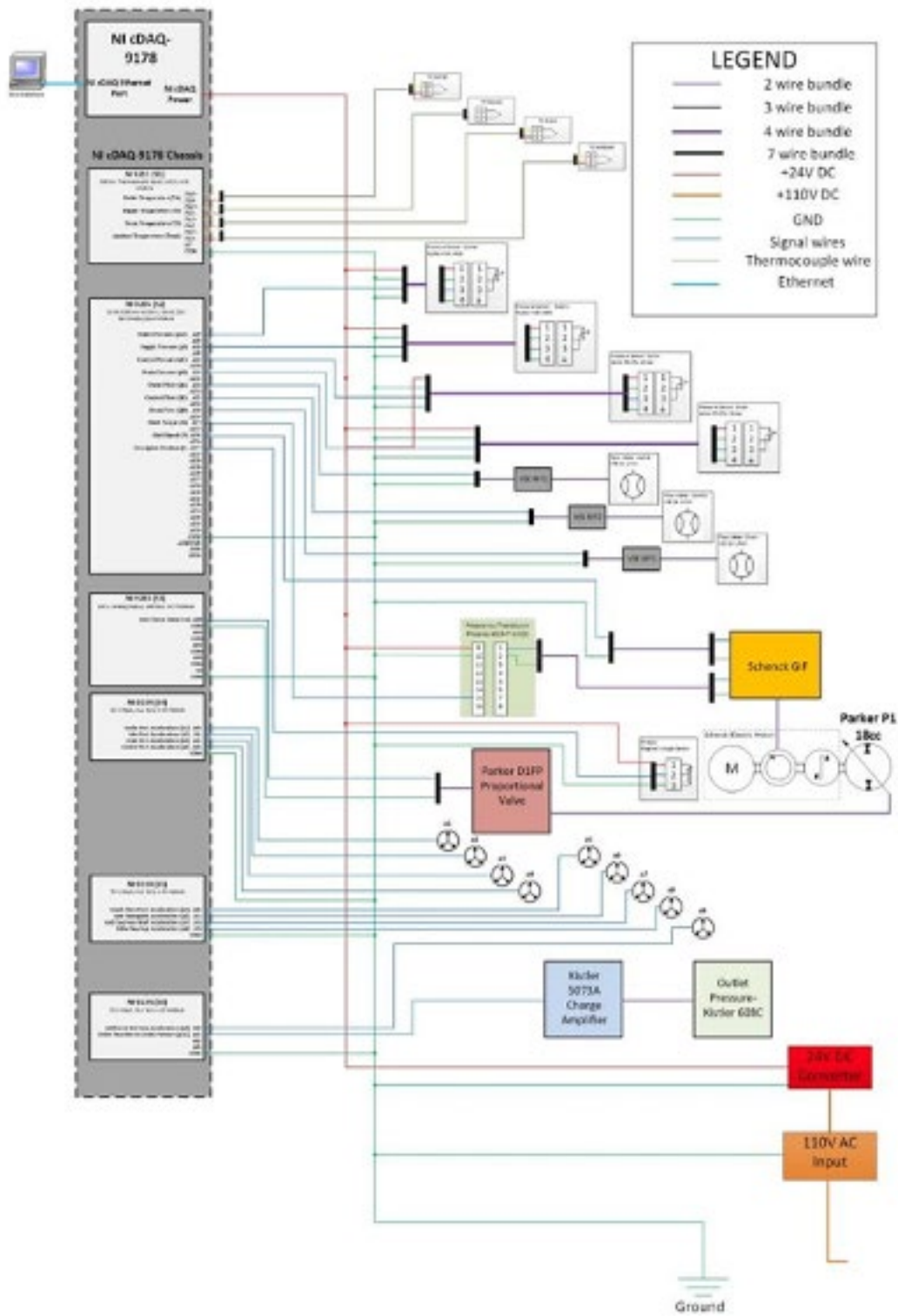


Figure 36: acquisition system wiring schematic

## 5.2 Experimental results

Different operating conditions have been taken into account. For each of those, the parameters listed in table iii have been acquired. In particular, all data have been acquired with a sampling frequency of 1kHz, except for the pressure ripple, which has been acquired with a 50kHz sampling frequency.

Examples of collected data are shown in figures 33 and 34.

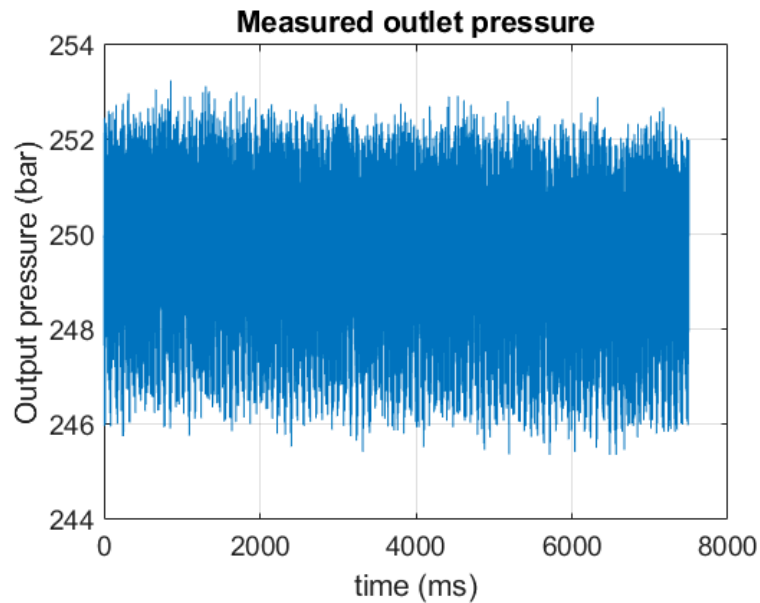


Figure 37: example of measured output pressure

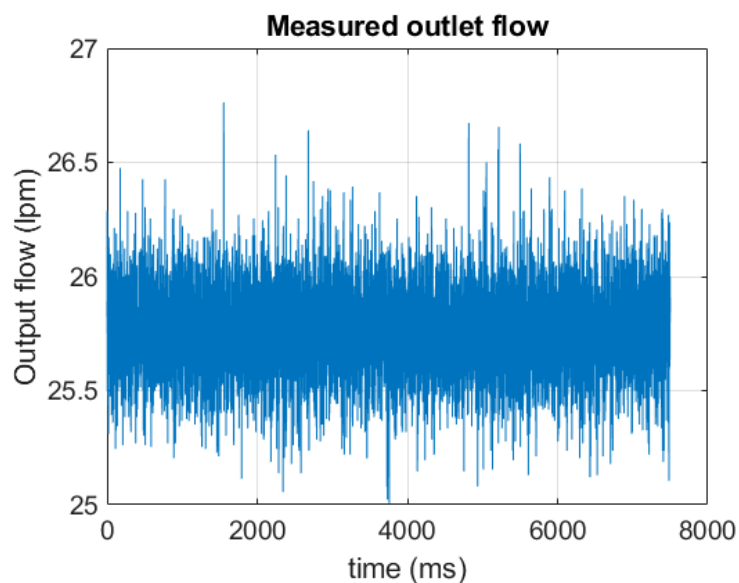


Figure 38: example of measured outlet flow

## 5.3 ISO 46 vs ISO 32 comparison

To observe how the oil viscosity affects the model results, the same test have been performed both with ISO 32 and ISO 46 oil. The differences between the 2 type of oil are shown in table 4.

	ISO 32	ISO 46
<i>Density (Kg/m<sup>3</sup>)</i>	850.8	861.519
<i>Viscosity (cSt)</i>	22.0133	30.3296
<i>Bulk modulus (Pa)</i>	$1.3581 \cdot 10^9$	$1.38484 \cdot 10^9$

Table 4: ISO 32 vs ISO 46 oil properties comparison

As first approximation, it has been observed that the differences between the drain flow and outlet flow are constant and related to the square root of density. This has been demonstrate experimentally by A.Sciancalepore starting from the orifice equation 16

$$Q = c_f \cdot A \cdot \sqrt{\frac{2 \cdot \Delta p}{\rho}} \quad (16)$$

From plot in figure 35, it is possible to notice that the flow discharge coefficient  $c_f$  is proportional to the square root of Reynolds number.

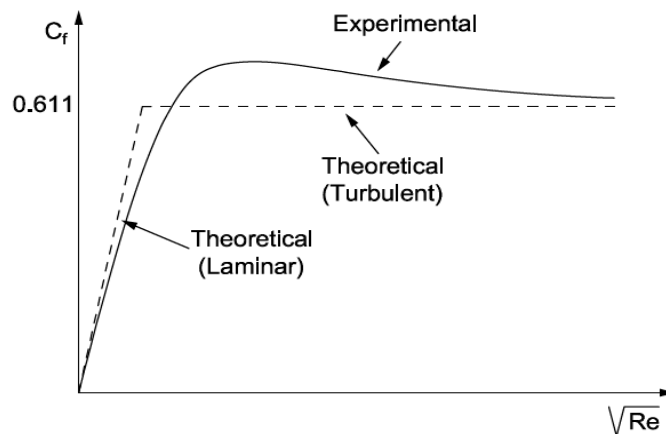


Figure 39: orifice flow coefficient vs square root of Reynolds number

Reynolds number, which is used to distinguish between turbulent and laminar fluid flow, is related to viscosity, conduct diameter, speed of the fluid and fluid density, as in equation 17

$$Re = \frac{v \cdot D}{\nu} = \frac{\rho \cdot v \cdot D}{\mu} \quad (17)$$

Considering that the flow across an orifice is directly proportional to the flow coefficient  $c_f$ , and that the flow coefficient is proportional to the square root of Reynolds number, it is possible to write this relation as in eq 18.

$$Q \propto \sqrt{Re} \quad (18)$$

From equation 18, it possible to see that the Reynolds number is inversely proportional to viscosity.

As conclusion, the output pump flow for 2 different oils will be equal to the square root of the inverse of their viscosity.

This relation can be written as in eq. 19

$$\frac{Q_{out,32}}{Q_{out,46}} = \sqrt{\frac{\rho_{46}}{\rho_{32}}} \quad (19)$$

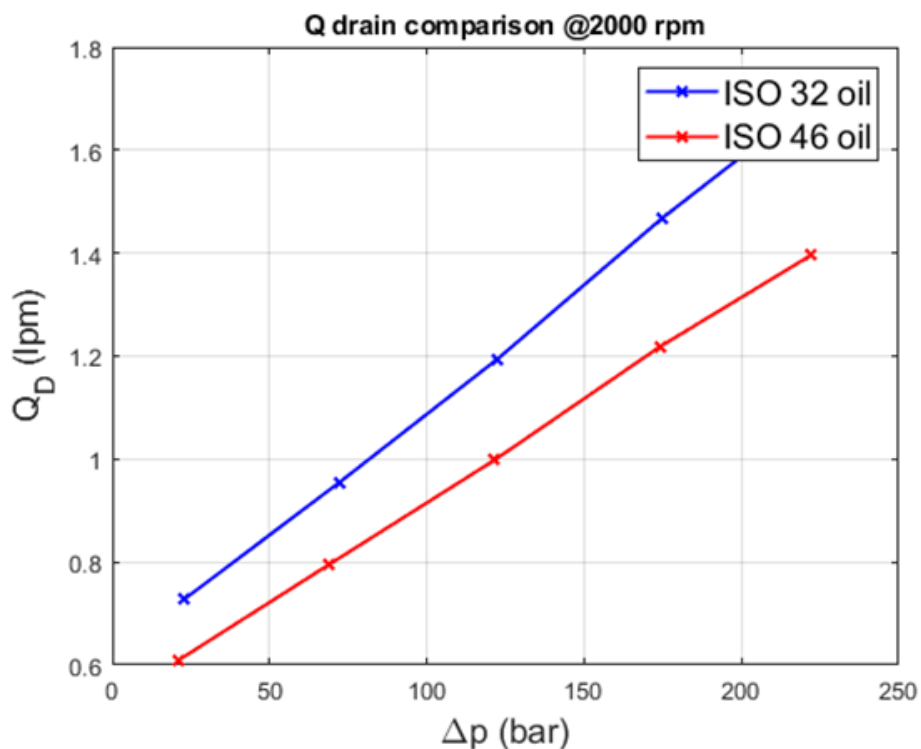


Figure 40: drain flow comparison for different oil types

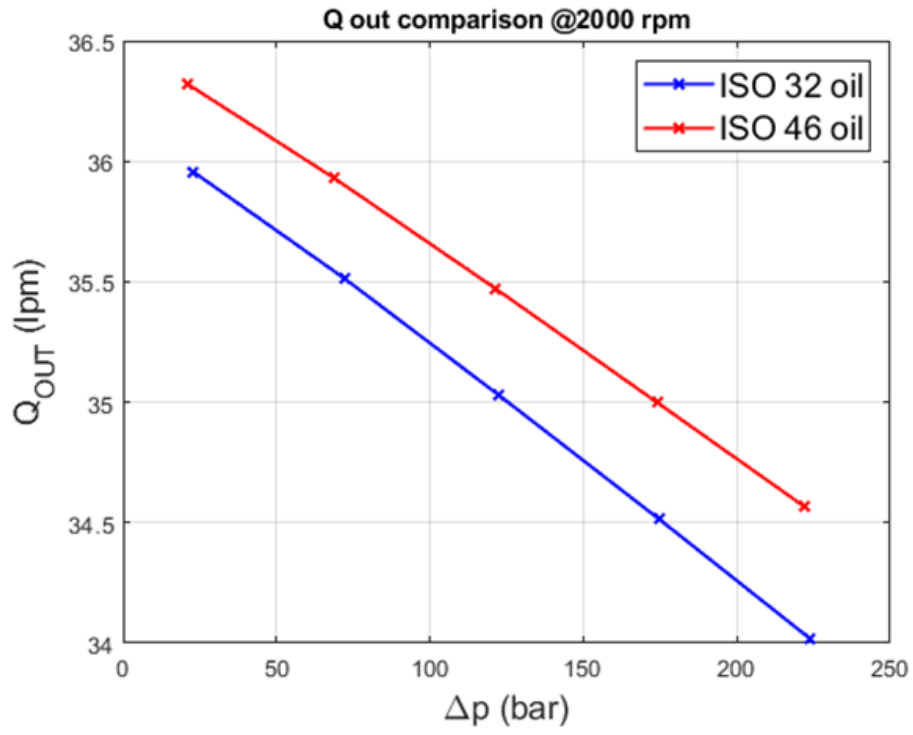


Figure 41: Output flow comparison for different oil types

## 5.4 Pressure ripple comparison

Interesting differences have been noticed between the measured healthy pressure ripple and the unhealthy one. In particular, different peak magnitude in frequency domain, which is related to different peak to peak values in time domain. Some measurements have been shown in figures 38 and 39.

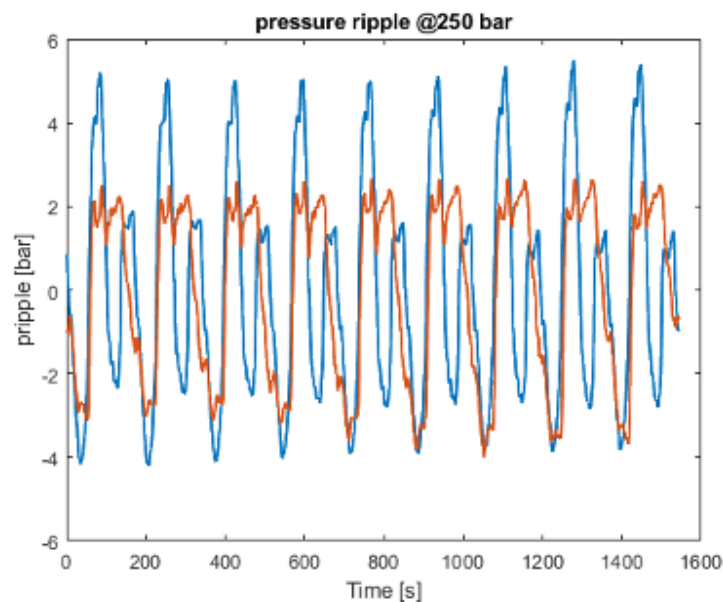


Figure 42: pressure ripple magnitude comparison

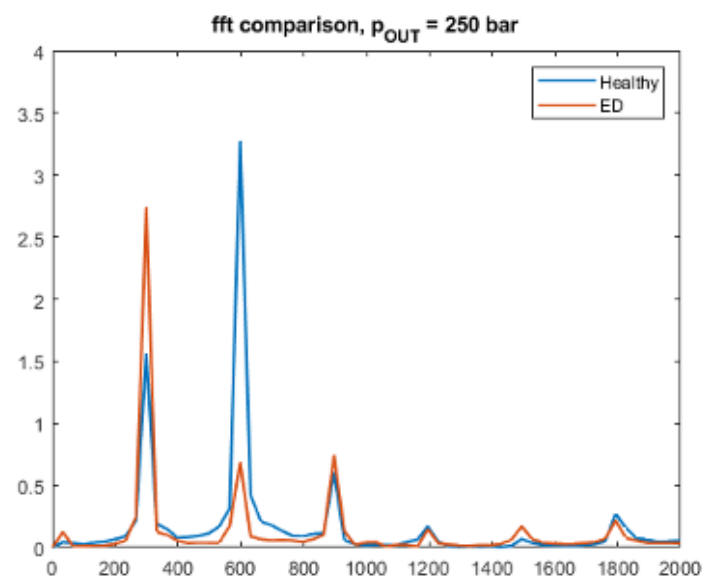


Figure 43: pressure ripple fft comparison

From figure 38, it is possible to observe that a 2000 Hz pressure sensor can be used to detect the first 3 peaks: in fact, to have a correct data acquisition (without aliasing), it is necessary to sample at least at 2 times the desired sampling frequency. This is better known as Nyquist's theorem. It will be better explained in appendix 3.

In figure 39 it is possible to understand the differences seen in fft plot: the healthy signal (blue line), has one peak very much higher with respect to the other one.

This behaviour is supposed to be related to different transition areas between high pressure and low pressure. To double check this hypothesis, further analysis on the valveplate would be required.

However, because of lack of time and because perfectly modelling the valveplate area is out of this research scope, the optical profilometer analysis has been indicated as future work

# 6 MODEL RESULTS AND VALIDATION

## 6.1 Drain flow

In this part, output flow, drain flow and drain pressure results and validation will be shown. Output pressure has been set by tuning the load orifice area: a recursive procedure has been applied in order to match the requested output pressure.

### 6.1 Drain flow

The drain flow has been assumed as proportional to speed, inlet pressure and outlet pressure. The percentage error with respect to the measured flow is shown in figure 41 and 43. Validation of this approach is shown in figure 45.

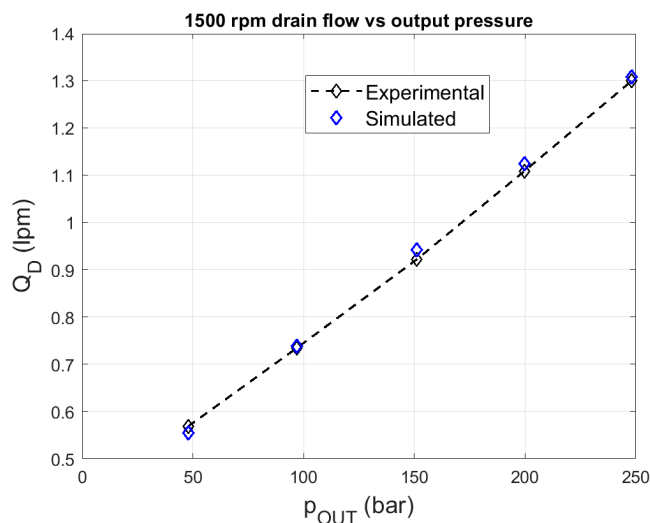


Figure 45: drain flow vs outlet pressure, 1500 rpm

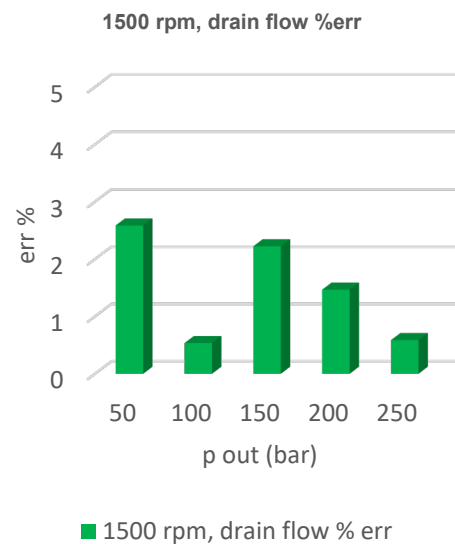


Figure 44: drain flow error, 1500 rpm

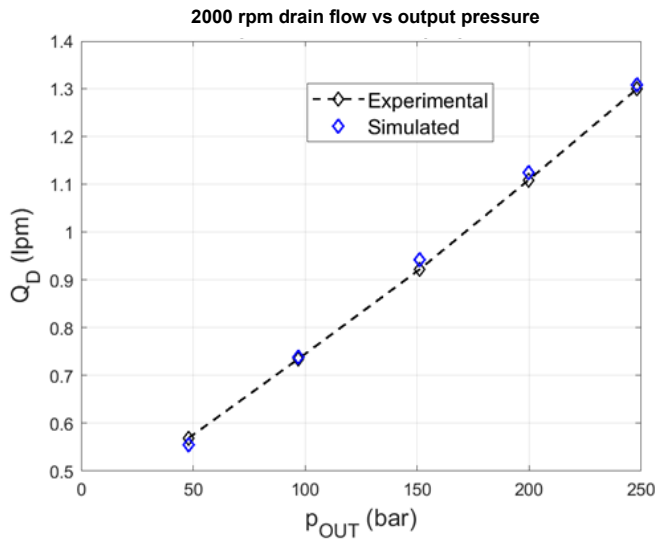


Figure 47: drain flow vs outlet pressure, 2000 rpm

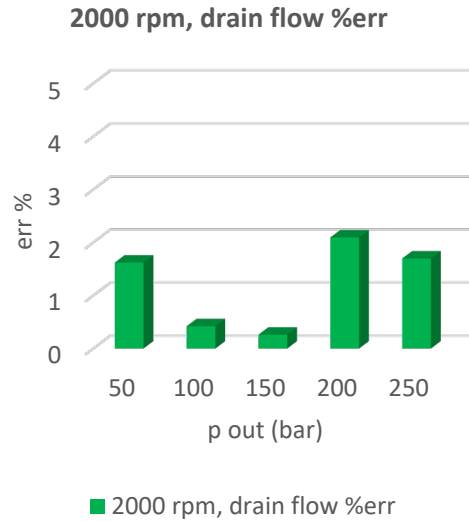


Figure 46: drain flow error, 2000 rpm

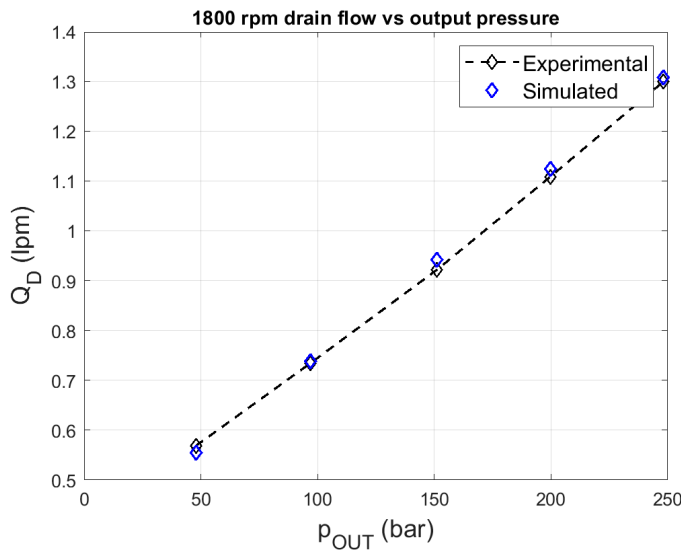


Figure 49: drain flow vs outlet pressure, 1800 rpm

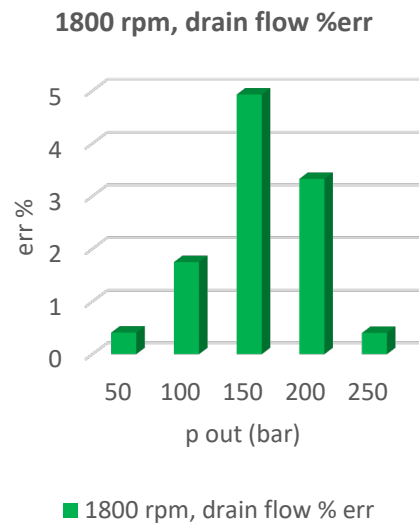


Figure 48: drain flow error, 1800 rpm

The error is always less than 5%. Thus the model is considered validated and quite precise from 1500 up to 2000 rpm. Those range has been chosen because they are the typical operating speed for an excavator. This will lead to the possibility of future work improvement and implementation on a real machine.

The error is not correlated to the output pressure. This is because the optimization algorithm looked for the smallest global error, not related to pressure.

## 6.2 Outlet flow

The outlet flow is shown in figures 46, 48, and 50

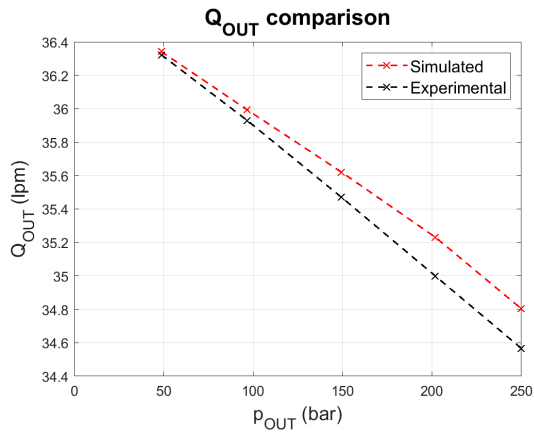


Figure 51: outlet flow vs outlet pressure, 1500 rpm

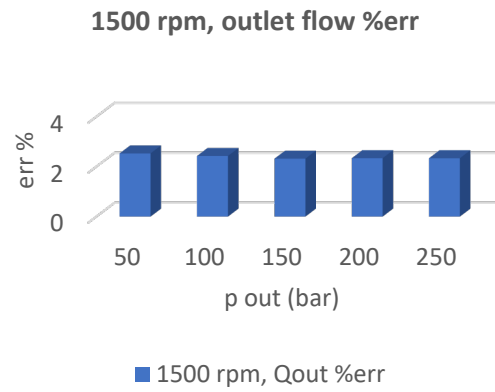


Figure 50: output flow error, 1500 rpm

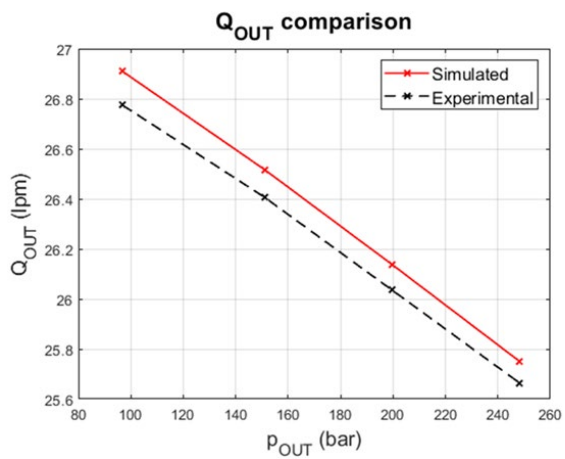


Figure 53: outlet flow vs outlet pressure, 1800 rpm

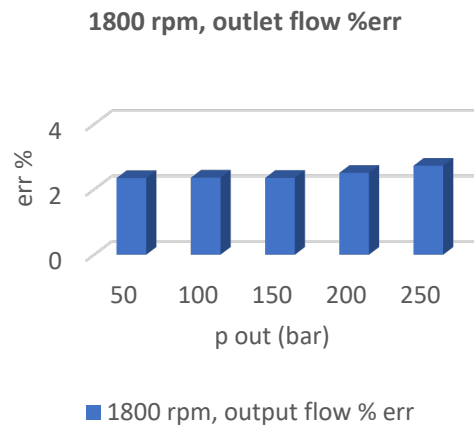


Figure 52: outlet flow error, 1800 rpm

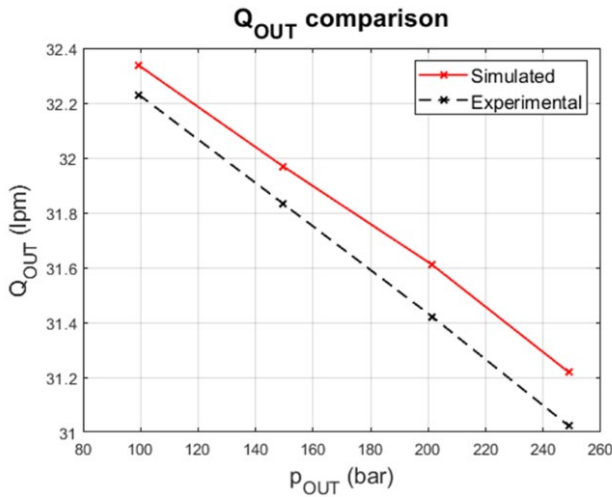


Figure 55: output flow vs output pressure, 2000 rpm

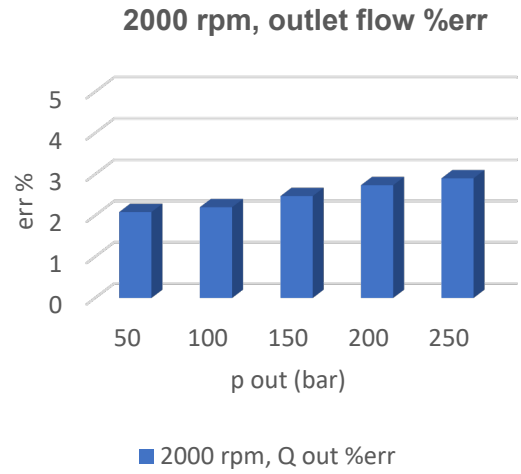


Figure 54: output flow model error, 2000 rpm

## 6.3 Drain pressure

To estimate the drain pressure, an optimization problem, similar to the one used to estimate the drain flow. Here the cost function, shown in equation 20 is the minimization of RSME, that is the square root of the squared error between the measured value and the simulated one.

$$C = \min \sum_{i=1}^N \frac{1}{N} \cdot \sqrt{\left( \frac{p_{Dmeas} - p_{Dsim}}{p_{Dmeas}} \right)^2} \quad (20)$$

Drain pressure validation will be shown together with the extremely damage validation paragraph.

## 6.4 Extreme damage model validation

To simulate the valve plate scratch, shown in figure 52, two different changes have been done to the healthy model.

First of all, the area file has been modified, in correspondence of the scratched part. Plus, an additional orifice has been added to the model, in order to simulate the flow path from the high pressure port toward the pump case.

To modify the area file, AVAS tool has been used using a damaged valve plate CAD instead of the healthy one (Figure 54).



Figure 57: extremely damaged valveplate

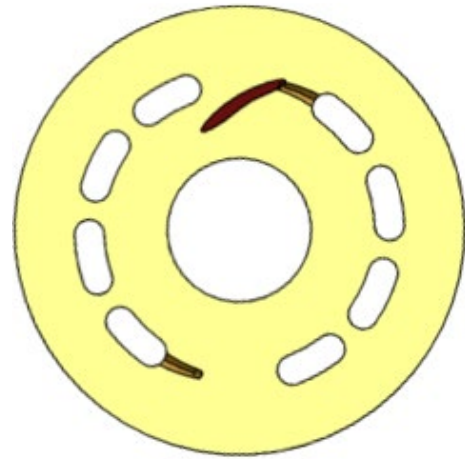


Figure 56: extremely damaged valveplate CAD

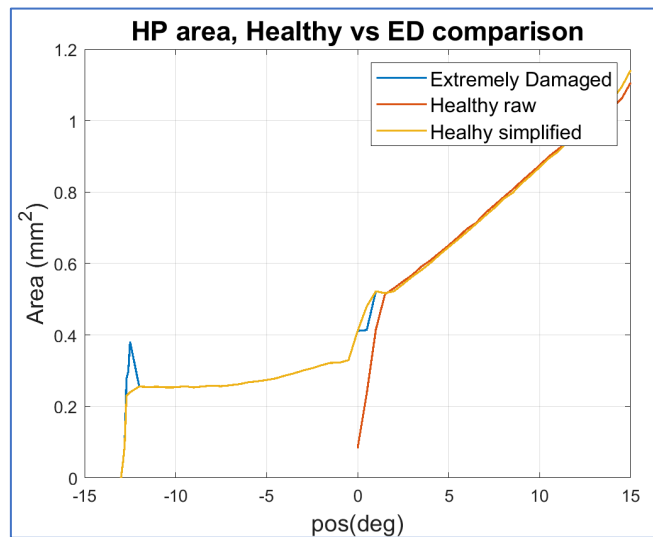


Figure 58: comparison between healthy and unhealthy groove area

The orifice area has been taken from the Avas output. As double check, an optimization problem has been set: assuming that the orifice flow coefficient is 0.65, the RSME between estimated flow and experimental flow has been minimized.

As conclusion, it has been observed that the optimal area is very similar to the AVAS tool one. However, a large error has been observed at low and medium pressures (50 and 100 bars), as shown in figure 55

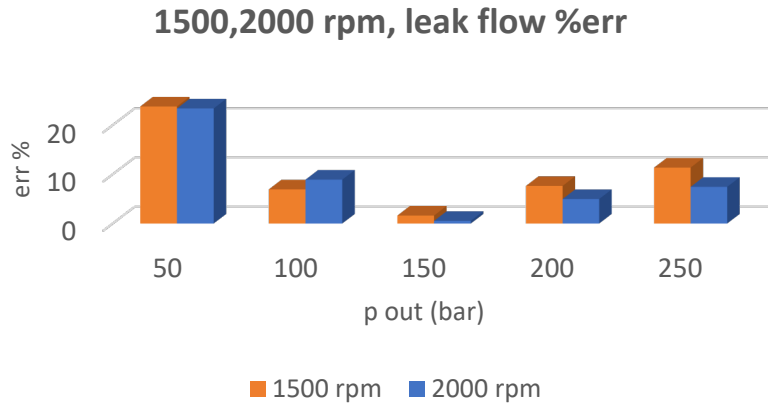


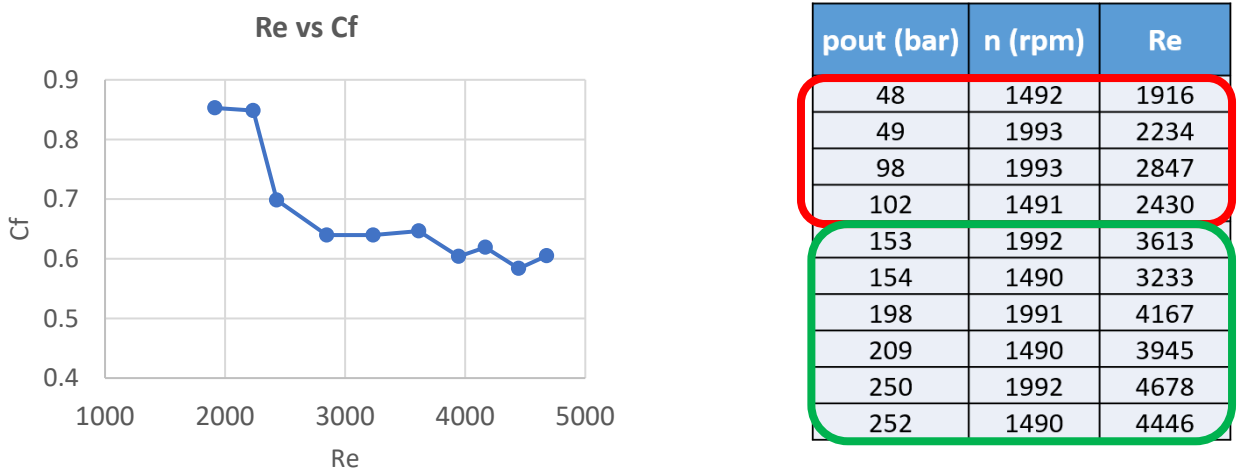
Figure 59: leakage flow error

At this point, it has been decided to investigate more about the flow coefficient. Keeping the orifice area fixed, the flow coefficient has been estimated. Then those values have been plotted with respect to the Reynolds number, to better investigate the orifice behavior (figure 56).

This number, identified as the ratio between the inertia forces over the viscous ones. At low values, the flow is laminar, while at high ones is turbulent. Reynold number is shown in formula 21

$$Re = \frac{\rho \cdot v \cdot D}{\mu} = \frac{\rho \cdot \frac{Q}{A} \cdot D}{\mu} = \frac{\rho \cdot Q \cdot \frac{4}{\pi D^2} \cdot D}{\mu} = \frac{\rho \cdot Q \cdot \frac{4}{\pi \cdot d}}{\mu} \quad (21)$$

Where  $\rho$  is the viscosity,  $v$  is the fluid speed,  $D$  is the passage area diameter,  $\mu$  is the dynamic viscosity and  $Q$  is the flow rate flowing across the orifice (difference between healthy drain flow and Extremely damaged valveplate drain flow).



pout (bar)	n (rpm)	Re
48	1492	1916
49	1993	2234
98	1993	2847
102	1491	2430
153	1992	3613
154	1490	3233
198	1991	4167
209	1490	3945
250	1992	4678
252	1490	4446

Figure 60: Comparison between Reynolds number and flow coefficient for exp. data

Viscosity has been computed from the case temperature. The empirical relation between those 2 variables has been found by collecting different temperature values and their respective density values, taken from Simscape Hydraulic fluid library. Then the best fitting line has been computed. This method is shown in figure 57.

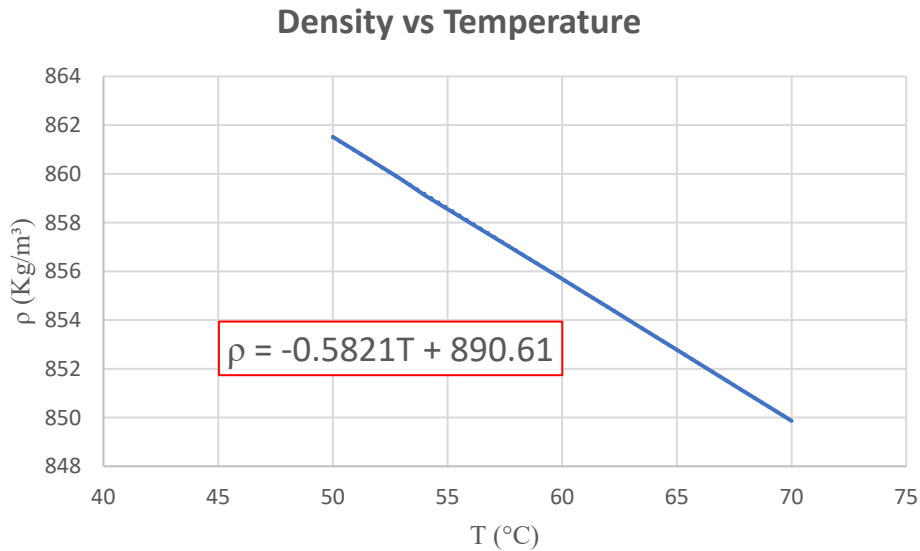


Figure 61: density vs temperature plot

The same above procedure has been used to determine the relation between temperature and dynamic viscosity (figure 58).

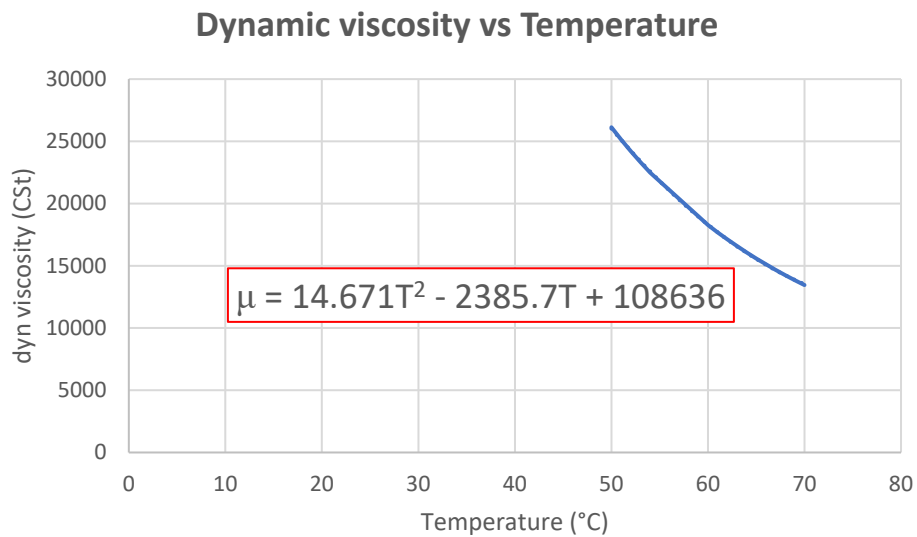


Figure 62: viscosity vs temperature plot

As precautionary decision, the model has been considered validated only at 150, 200 and 250 bars. For this condition, the flow coefficient has been assumed equal to 0.62, because when the Reynolds number is greater than 2900 the flow is considered completely turbulent.

Figure 60 shows the model testing, using collected data at 1500 and 2000 rpm. Figure 61, instead, shows validation of the algorithm with data collected at intermediate speed (1800 rpm)

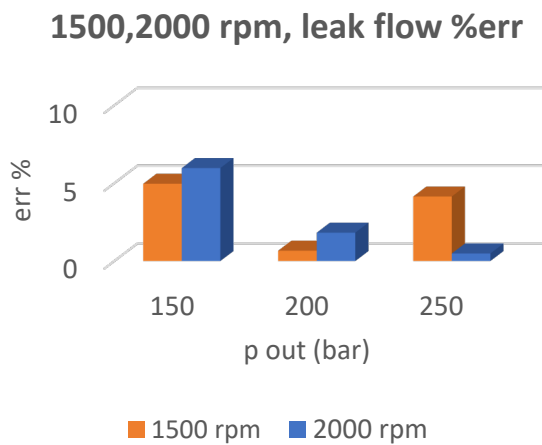


Figure 64: leakage flow model error

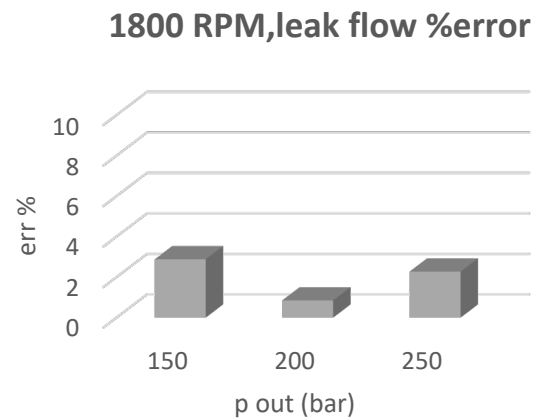


Figure 63:leakage flow error – validation at 1800 rpm

Since for the intermediate faults it will not be possible to know the leakage flow toward the scratch, the ratio between the Reynolds number and flow coefficient will be used as constraint. Solving the 2 equation systems (iii), it has been possible to compute the mathematical formulation of those value. It will depend only from known values (density, viscosity, output pressure and orifice area).

$$\begin{cases} Re = \frac{\rho \cdot v \cdot D}{\mu} \\ Q = c_f \cdot A \cdot \sqrt{\frac{2 \cdot \Delta p}{\rho}} \end{cases} \quad (22)$$

$$\frac{Re}{c_f} = \frac{\rho \cdot c_f \cdot \sqrt{\frac{2 \cdot \Delta p}{\rho}} \cdot D}{\mu} \quad (23)$$

$$\frac{\rho \cdot c_f \cdot \sqrt{\frac{2 \cdot \Delta p}{\rho}} \cdot D}{\mu} \geq \frac{2900}{0.62} \quad (24)$$

## 6.5 Drain pressure estimation

The drain pressure formula has been found from experimental data: after plotting the drain flow with respect to the drain pressure, the best fitting line has been computed. Figure 61 shows the experimental line (obtained from collected data at 1500 and 2000 rpm), the second degree fitting line and the validation data at 1800 rpm, both for healthy and for unhealthy conditions.

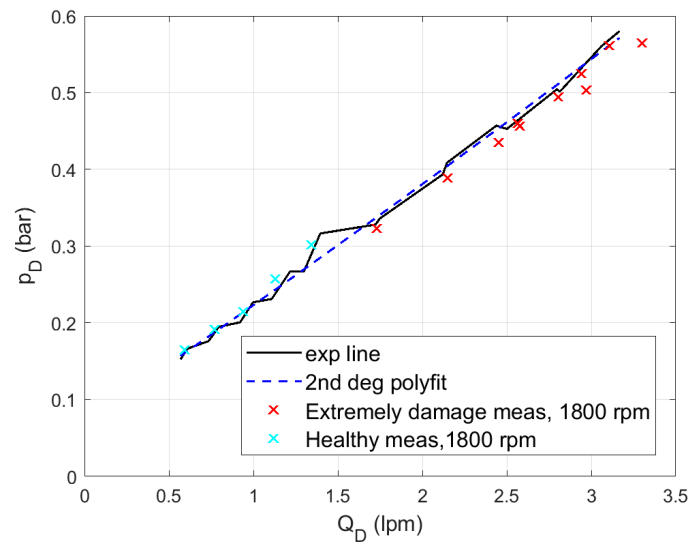


Figure 65: drain pressure vs drain flow, healthy and ED data

The error between the measured data and the estimated one, in extremely damaged (ED) valveplate experiments are shown in figure 62;

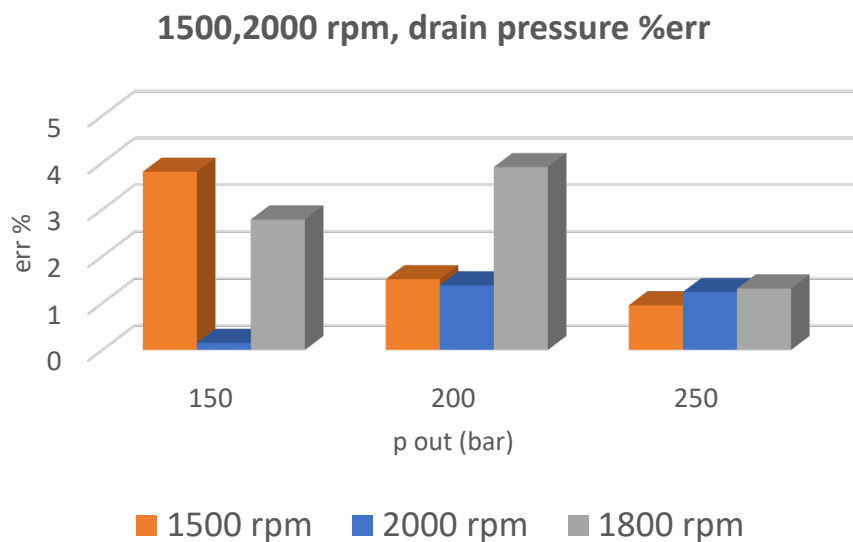


Figure 66: line model error, healthy and ED data

# 7 CONDITION MONITORING MODEL

A standard approach used to create efficient condition monitoring models is depicted in figure 63. The disadvantage of this method is related to the fact that a lot of experiment must be performed to get satisfactory results.

costly solution, because it requires a lot of time to prepare the experimental setup. Plus, some errors in experimental procedure can lead to wrong considerations.

In this thesis, an alternative approach shown in figure 64 will be used.

This approach will dramatically decrease the time to collect data: in fact, a digital twin lumped parameter model will be used.

Another advantage is that the physical components will not have to be damaged. That is crucial, because often internal pump components are very expensive and their availability is often limited.

The alternative procedure workflow is shown in figure 64

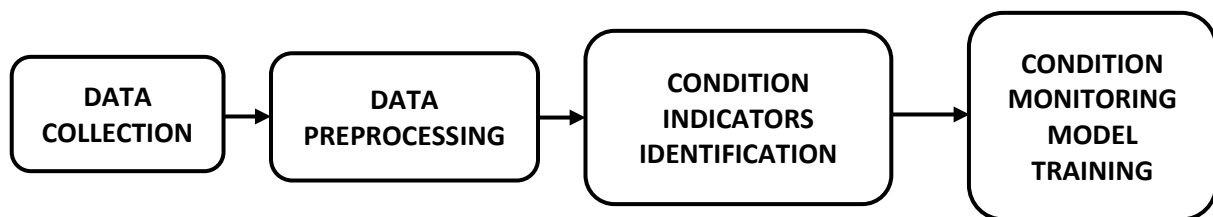


Figure 67: general condition monitoring model workflow

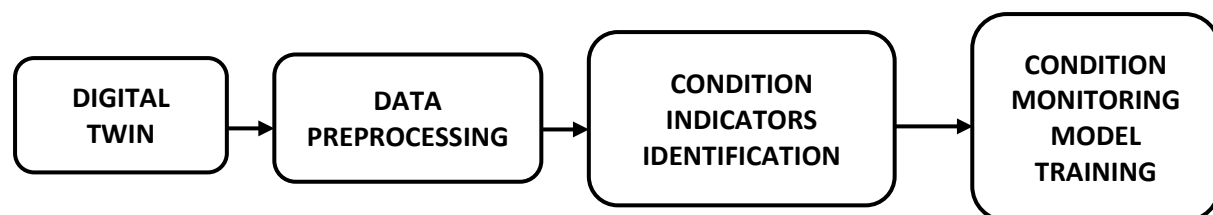


Figure 68: alternative condition monitoring model workflow

In this chapter, different algorithms will be presented and explained. Finally, the results will be compared and discussed. Then the best algorithm will be chosen.

## 7.1 Machine learning introduction

Machine learning algorithms can accomplish different variety of tasks, such as transcription, regression, machine translation, regression, denoising, density estimation, and classification.

An example of transcription task can be the OCR (optical character recognition) technology: the algorithm converts a scanned document in text format. Relatively to regression task, it consist in finding a function able to correlate a set of input and output values. An example of regression problem has been faced in previous chapter, during the estimation of the parameters which relates inlet pressure, outlet pressure, speed to drain flow.

Machine translation consist in converting symbols from one language to another one.

The last task is the one that has been set for the condition monitoring part. In fact, classification consist in identifying different classes (in this case, different fault levels) and assign the right class to every element of a given dataset.

Depending on the type of dataset, machine learning problems can be divided into supervised problem and unsupervised ones. The first ones are characterized by non-labeled data: that means that the algorithm cannot know the properties of each data. In case of condition monitoring, the dataset is labeled: every data is associated to different fault levels: healthy, extremely damaged, intermediate level, damaged piston, damaged slipper. The labeled data are organized in a design matrix, which will be fed into the condition monitoring model. An example of design matrix is the one in table iii, where H stands for healthy pump, ED for extremely damaged valveplate, ID for intermediate damage. CD, instead, is related to cylinder damage, SD is slipper damage.

All the mean value sensor data are collected. Plus, for the pressure ripple, variance value have been collected.

In table 5, due to space issues, the sensor names abbreviation are shown.

1. drain pressure ( $p_D$ )
2. drain flow ( $Q_D$ )
3. drain temperature ( $T_D$ )
4. outlet pressure ( $p_{out}$ )
5. outlet flow ( $Q_{out}$ )
6. outlet temperature ( $T_{out}$ )
7. inlet pressure ( $p_{in}$ )
8. inlet temperature ( $T_{in}$ )
9. displacement control flow ( $Q_C$ )
10. displacement control pressure ( $p_C$ )
11. displacement level ( $\beta$ )
12. pressure ripple variance ( $prippple_{VAR}$ )
13. Healthy condition (H)
14. Extremely damaged valveplate (ED)
15. Cylinder damage (CD)
16. Slipper damage (SD)

$p_D$	0.12
$Q_D$	0.57
$T_D$	65
$p_{out}$	47.9
$Q_{out}$	27.12
$T_{out}$	49.6
$p_{in}$	28.4
$T_{in}$	48.9
$Q_C$	0.28
$p_C$	24.5
$\beta$	1
$Prippple_{VAR}$	10.9
H	0
ED	0
CD	0
SD	1

Table 5: sensor name abbreviation

Before starting to consider the different proposed solutions, it is necessary to understand the differences between overfitting, underfitting and appropriate capacity. That can be understood by observing the figure 65 [20]

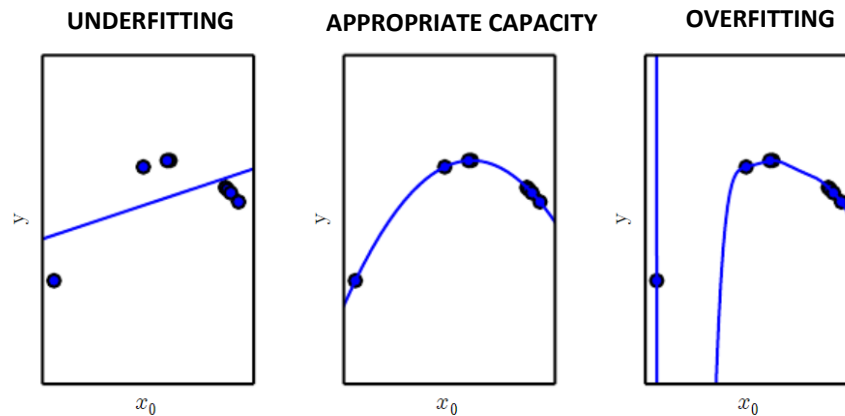


Figure 69: difference between underfitting, appropriate capacity and overfitting

In the first case, the model cannot fit the data trend (because the degree is too low). The central case represents the optimal solution: degree 2 is the optimal one to fit the parabolic trend. The last case is a clear example of overfitting: the degree 9 plot presents highly unwanted oscillating behavior.

## 7.2 Supervised learning models

### 7.2.1 Support vector machine (SVM)

This model is very useful to discriminate between different classes (i.e: faults levels). Originally, it was designed for binary classification problems. When the classes are more than 2, the problem is divided into different binary classification sub-problems (one-to-one approach).

Another possible approach is the one-to-rest approach: one class is separated with respect to all the other ones.

SVM algorithm uses different hyperplanes to discriminate between different classes.

A simple example of one to one approach is shown in figure 66 [21]

Figure 67 [21], instead, shows a one to rest approach.

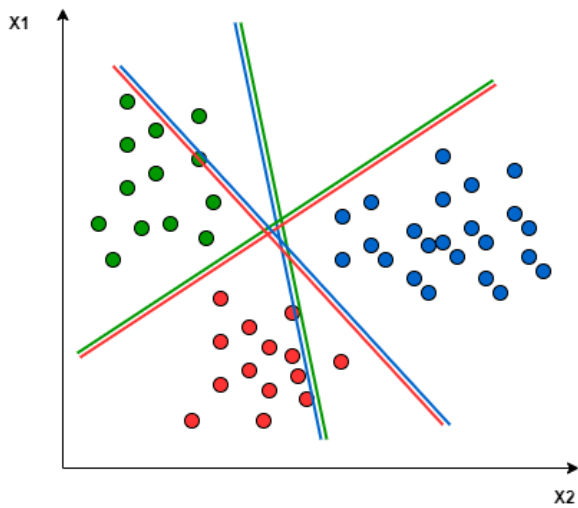


Figure 71:one to one SVM approach

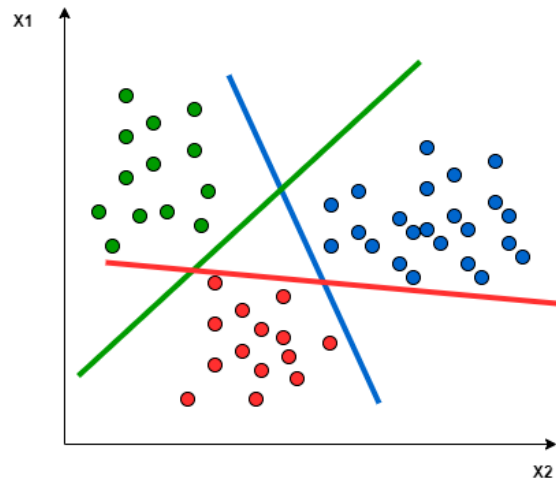


Figure 70:one to rest SVM approach

Since the hyperplanes are linear, sometimes the problem can be more complex, as in figure 68 [21].In this case, a linear hyperplane in xy space cannot be used.Thus, the kernel trick is introduced: a new dimension is add.For example, in figure 69[21] , a kernel with equation  $z^2 = x^2 + y^2$  has been used.In xz plan the distinction becomes quite straight forward.

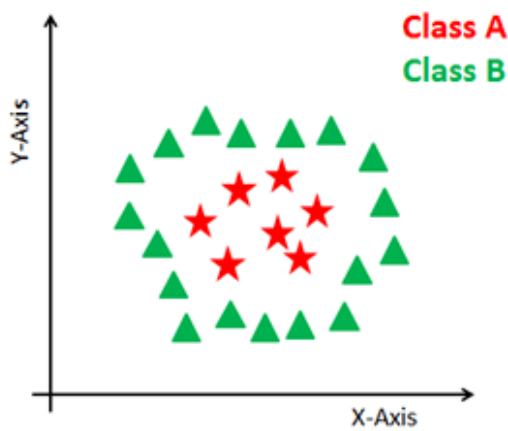


Figure 72: classification problem in xy plane

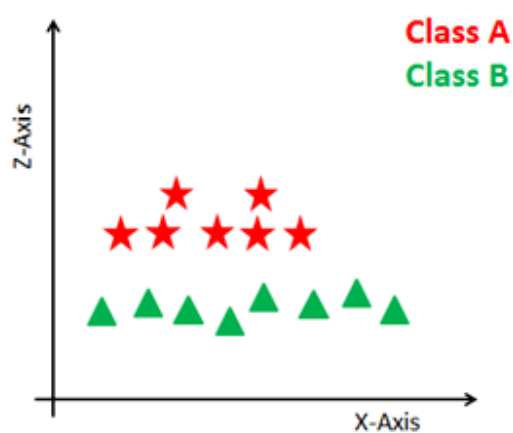


Figure 73:classification problem in xz plane

The last example is depicted in figure 70, taken by Coursera online platform.

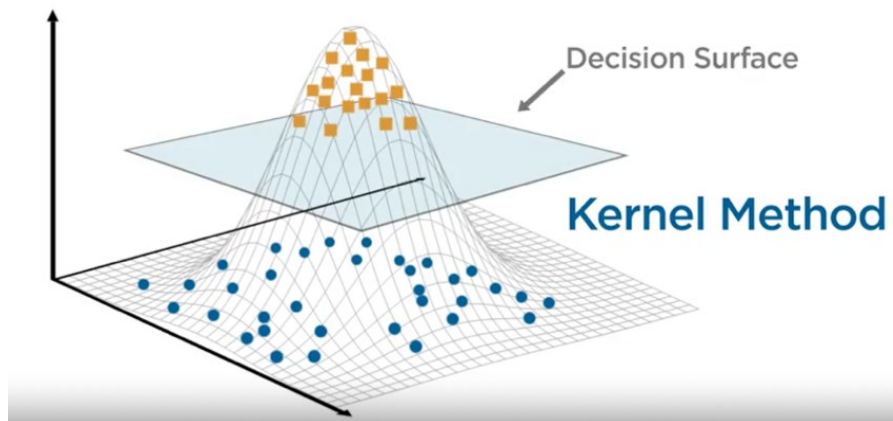


Figure 74: kernel method representation

### 7.2.2 K-nearest neighbor

This algorithm is very accurate for high training set values, but at the very same time is computationally expensive. Its weak point is that the algorithm cannot learn that one feature is more discriminative with respect to another one.

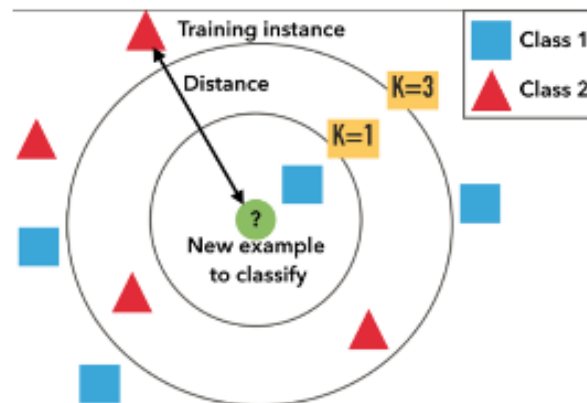


Figure 75; k-nn problem representation

This algorithm computes the distance between the new example to classify and the neighbor points, which can be part either of a class or of another one. Those distances are saved into a matrix, and are labeled with the class type (i.e : square or triangle).

The matrix is ordered by sorting the distance in ascendant order, that is , smaller to higher.

The k rows of this matrix are considered. The most frequent class label is assigned to the example data.

Depending on solvers, the distance can be computed as Euclidean one, that can be interpreted as the cathet of a triangle, or Manhattan distance, which corresponds to the sum of the 2 perpendicular sides of a triangle.

Figure 72[22] helps to better understand the differences between the 2 possible distances.

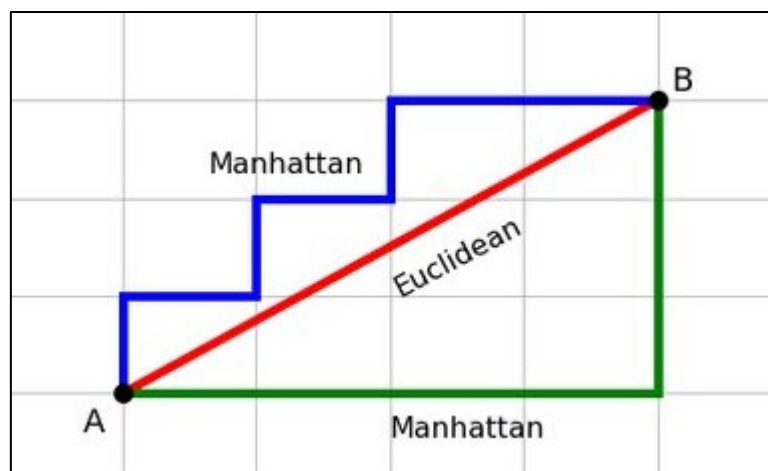


Figure 76: Manhattan vs Euclidean distance

### 7.2.3 Decision tree

This algorithm can be represented by a tree in which the branches are feature (pressure, temperature and so on), while the leaves are class labels (healthy, Extremely damaged).

To better understand the working principle, a decision tree is shown in figure 72

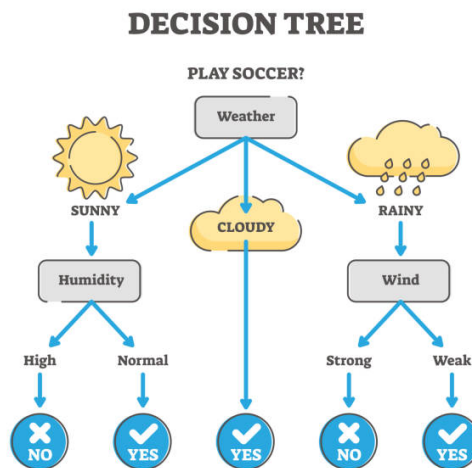


Figure 77: decision tree example

The root node, that is the starting one, is chosen by minimizing the entropy and information gain or minimizing the Gini impurity.

Entropy can be defined as quantity of randomness of a certain variable. If this value is high, then the decision tree will not be able to clearly distinguish between different situations.

It is obtained by using the formula 25

$$H(X) = - \sum_{i=1}^n P(x_i) \log_b P(x_i) \quad (25)$$

Information gain is the amount of information obtained by a random variable by observing another random variable. It is an index that shows how much a changing in one variable affects another one.

Basically, it is the difference between the entropy of parent node and weighted average entropy of child nodes. It can be expressed by formula 26

$$IG(S, A) = H(S) - \sum_{i=0}^n p(x) \cdot H(x) \quad (26)$$

Entropy and Information gain are used in ID3 (Iterative Dichotomiser 3) type classification learner algorithm.

The Gini impurity value is used instead in CART (Classification and Regression Tree) problem. It can be interpreted as the probability of misclassifying an observation. This index can have

values from zero to one. A value of 0 means that there is no misclassification (ideal case). The Gini impurity for a number  $n$  of different classes can be represented as follows

$$Gin_x = p_1 \cdot (1 - p_1) + p_2 \cdot (1 - p_2) + \dots + p_n \cdot (1 - p_n) \quad (27)$$

With

$$\sum_n^{i=1} p_i = 1 \text{ or } \sum_{j \neq i} p_j = 1 - p_i \quad (28)$$

Then

$$Gin_x = \sum_n^{i=1} p_i \cdot \sum_{j \neq i} p_j = \sum_n^{i=1} p_i \cdot (1 - p_i) \quad (29)$$

# 8 CONDITION MONITORING RESULTS

## 8.1 Test 1: Healthy / Unhealthy Detection

### 8.1.1 Steady state values only

In this first test, only a distinction between healthy and unhealthy pump has been implemented, to show different advantages and limits of this approach. After having taken into account different algorithms, quadratic SVM has been used. Using outlet flow, drain flow, output pressure, drain pressure, velocity the obtained accuracy is about 95%, as it is possible to observe in figure 74. Class 1 is referred to faulty pump, while class 0 is the healthy pump class indicator.

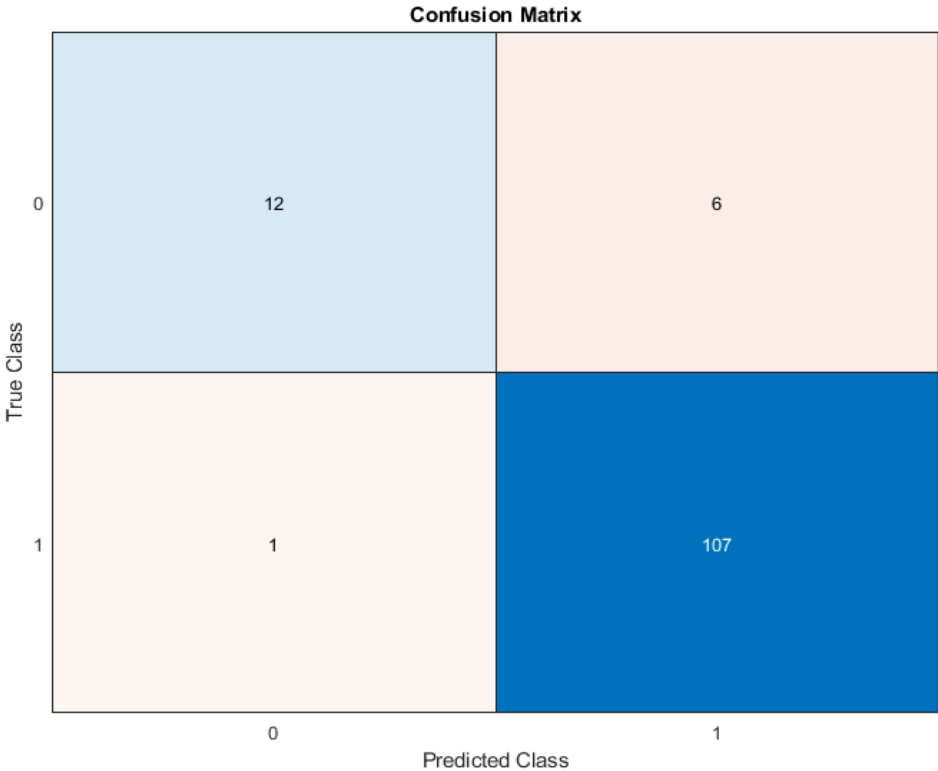


Figure 78: confusion matrix

In this case, 12 class 0 samples have been correctly identified as healthy, while 107 samples have been correctly identified as unhealthy. 1 sample has been classified wrongly as healthy and 6 samples have been wrongly classified as healthy.

Thus, the number of uncorrected classified samples is 7, over a total population of 126 samples. This correspond to 94.4% of model accuracy.

For research purposes, only drain pressure sensor, outlet pressure sensor and speed have been considered in another test. This choice is motivated by the high price of flow meter sensors.

The obtained accuracy is 85%.

In particular, it has been noticed that the slipper damage can lead to uncorrected predictions: in fact, the drain flow will be very near to the healthy pump condition. This is because this kind of leakage has a very small effect on the pump flow, since the orifice area .The figure iii better explain this issue. The confusion matrix in figure iii is used to better investigate the limit of this first approach.

To improve algorithm accuracy, in the next paragraph pressure ripple will be taken into account.

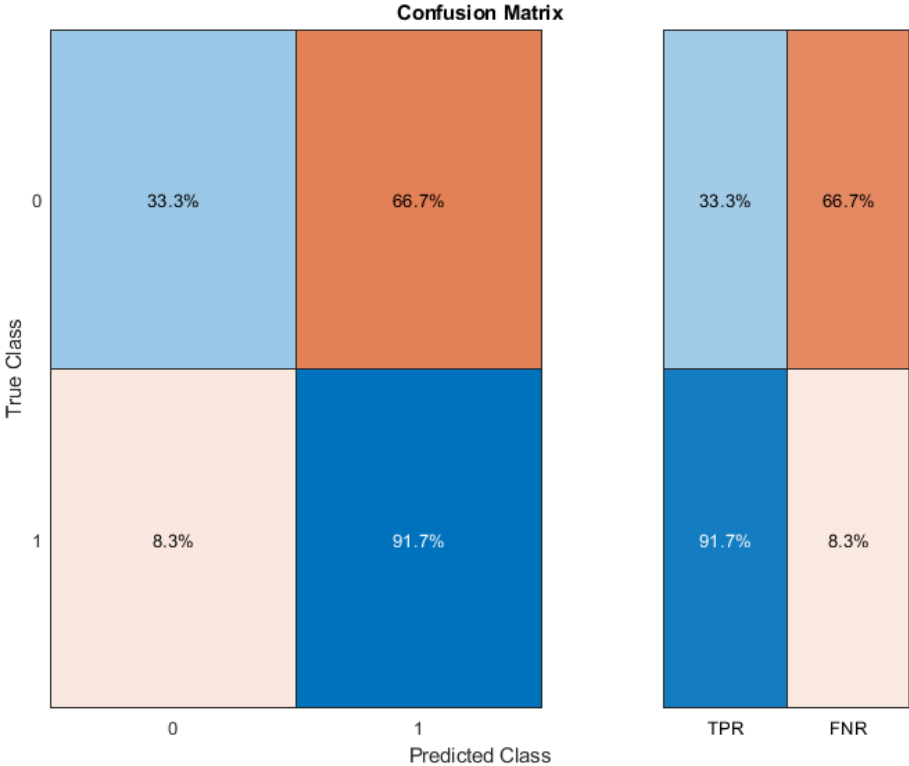


Figure 79: confusion matrix for test 1a

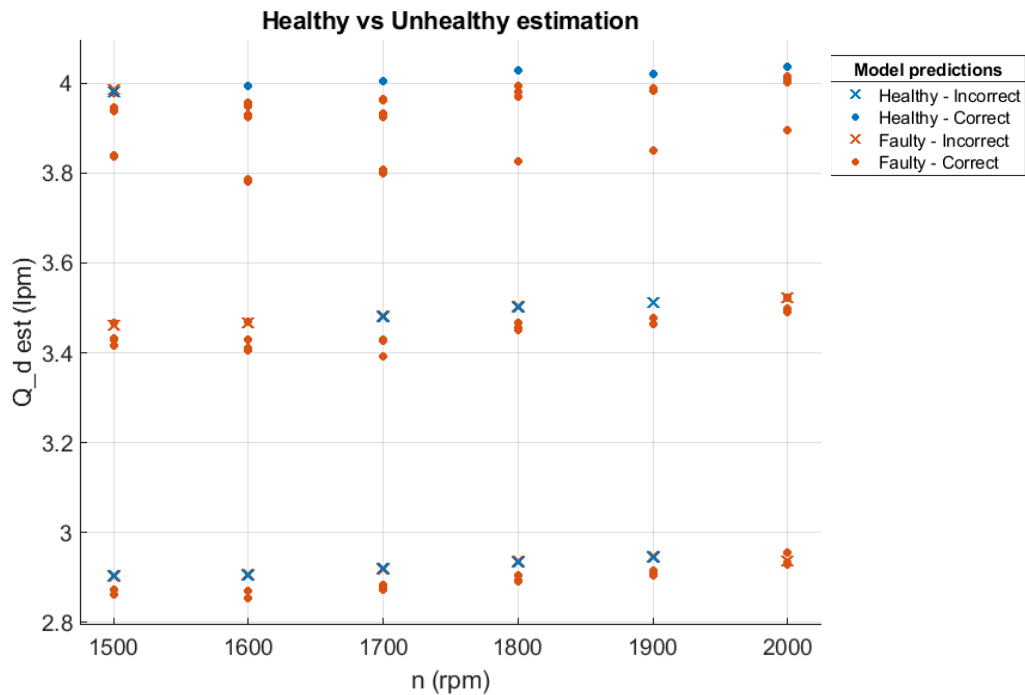


Figure 80: speed vs estimated drain flow

The confusion matrix in figure 79 is composed by 4 squares. The first one shows the case in which the true class 0 (real healthy data) is correctly predicted by the algorithm. In 66.7% of cases, the healthy data is interpreted as unhealthy (because the algorithm is not able to distinguish between slipper damage and healthy pump). In 91.7% of cases the fault is correctly predicted, while in 8.3% the condition monitoring model is classifying faulty data as healthy.

### 8.1.2 Pressure ripple variance only

The variance can be defined as in formula iii. It indicates the squared deviation of a variable from its mean value.

$$\sigma^2 = \frac{\Sigma(X - \mu)^2}{N} \quad (30)$$

Where  $\sigma^2$  is the population variance,  $\Sigma$  is the sum operator,  $X$  is a random value taken from population,  $\mu$  is the population mean and  $N$  is the total number of population samples.

From experimental results showed in previous chapter, it has been seen that the healthy pressure ripple is very different with respect to the faulty one.

To understand how the pressure ripple sensor can improve the model accuracy, a test considering only this parameter has been performed. The confusion matrix in figure 77 shows that using a medium K-nn algorithm, it is possible to obtain a quite satisfying

result (83%). However, the number of samples incorrectly identified as damaged is high: this is not acceptable, because a false alarm means a not necessary stop of the equipment. This issue can lead to severe money losses.

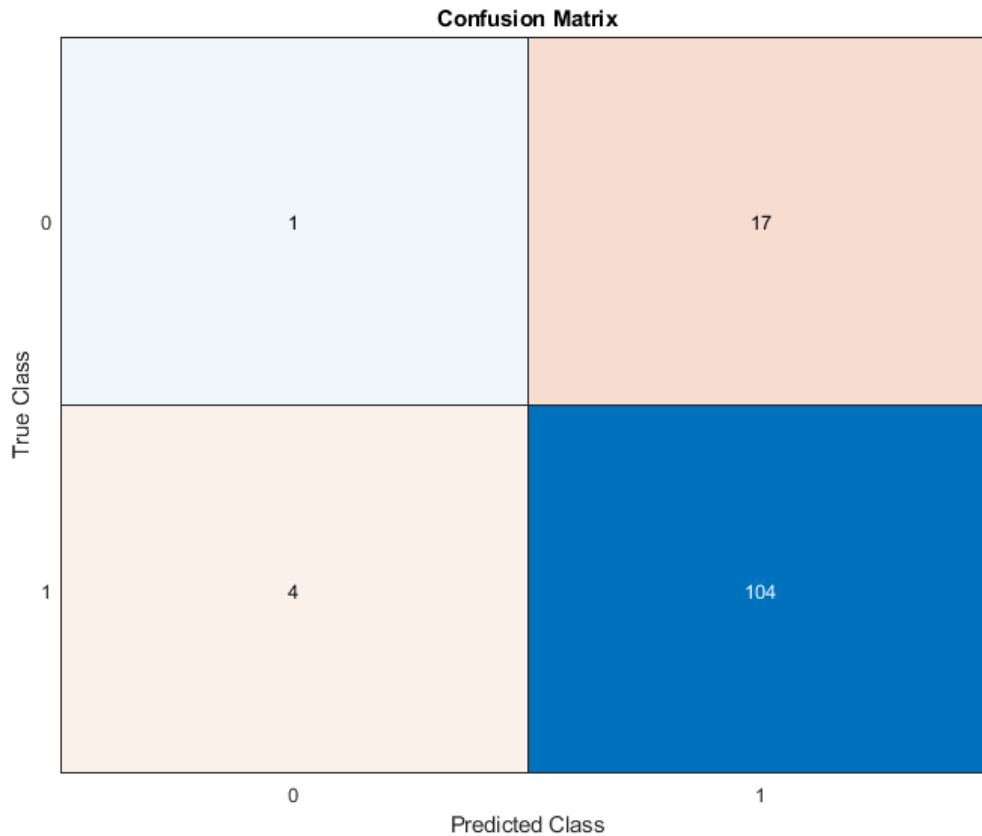


Figure 81: confusion matrix for test 1b

From figure 61, it is possible to see that one over 18 healthy sample is correctly detected, while 17 samples are wrongly identified as damage conditions. 104 samples over 108 are correctly detected as unhealthy, while 4 unhealthy observers are incorrectly classified as healthy.

### ***8.1.3 Steady state values and pressure ripple variance***

In this case, the model has reached a value of accuracy of 91%. Analyzing the confusion matrix, it is possible to observe that the model predicts in a very precise way the unhealthy data (118 samples over 126). Relatively to the healthy class, 13 samples over 18 are identified correctly.

A brief recap relative to the needed sensor, the optimal algorithm and the required sensors is shown in table 6.

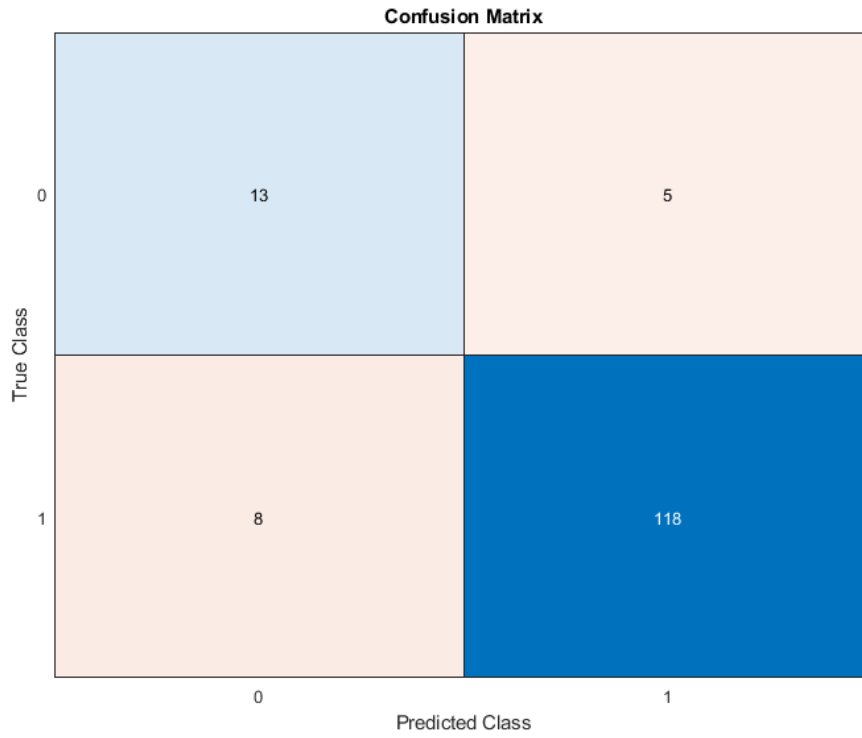


Figure 82: confusion matrix for test 1c

Algorithm	sensors	accuracy
<b>Quadratic SVM</b>	$p_d, n, p_{out}$	85%
<b>Quadratic SVM</b>	$p_{Ripple}$	83%
<b>Cubic SVM</b>	$p_d, n, p_{out}, p_{ripple}$	91%

Table 6: test 1 model results

# 8.2 Test 2: Different Damages, No Combination

In this test, different types of damages have been taken into account (cylinder damage, slipper damage, valveplate damage). Only one damage per time has been considered. The best condition monitoring algorithm has been shown.

The used sensor are drain pressure, pressure ripple variance, output pressure and speed.

Using a quadratic SVM algorithm an 85% accuracy has been obtained.

The most critical damage to detect is the slipper damage. In fact, as it is possible to observe in figure 79, only 61% of the slipper damage data are correctly classified.

The cause of this bias is probably due to a too small fault, which need to be better modeled to be predicted successfully.

Healthy case is correctly detected in 83.3% of cases. In the other cases is wrongly classified as slipper damage.

Extreme damage is predicted well in 94.4% of cases. In 5.6% of cases is detected as healthy.

Finally, the model can predict with 94.4% of accuracy a damaged cylinder

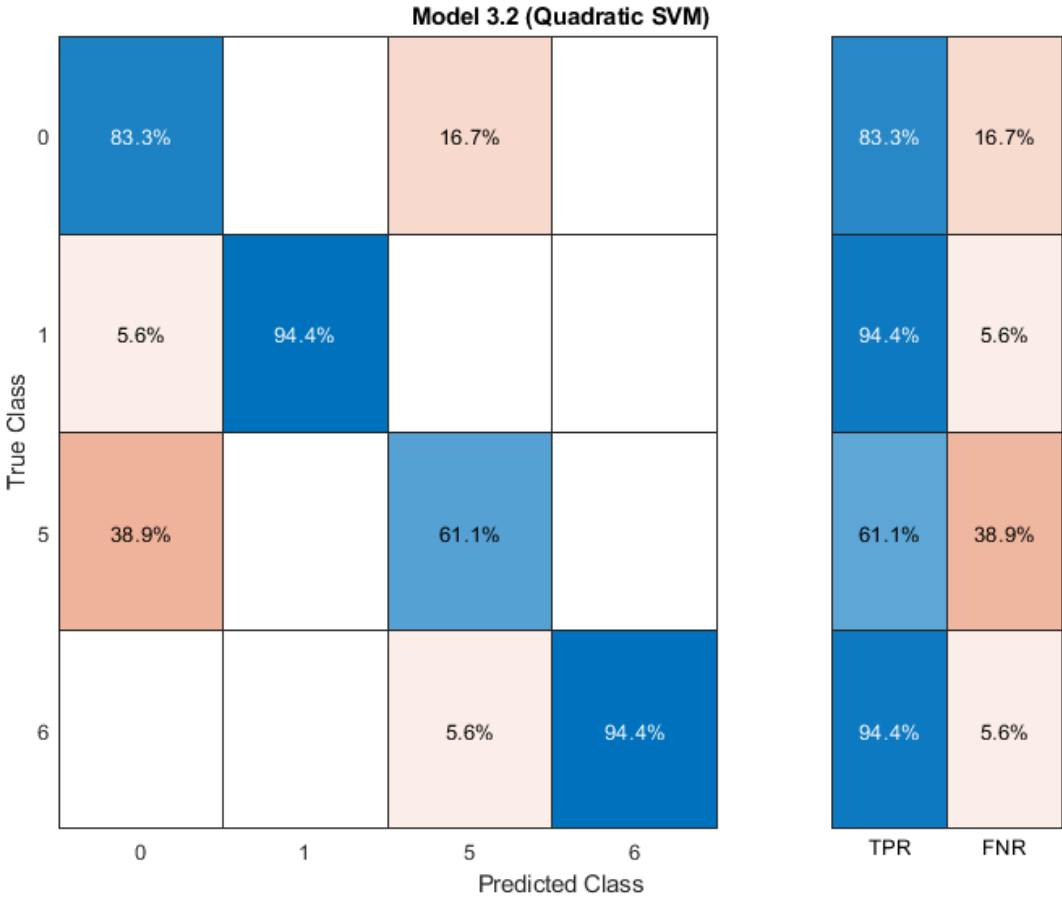


Figure 83: Confusion matrix test 2

The pie chart in figure 81,82,83,84 can better explain the algorithm limits.

■ Healthy   ■ ED valve plate   ■ Slipper fault   ■ Cyl Fault

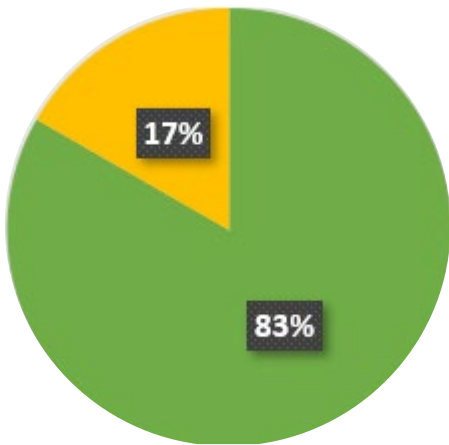


Figure 87: class 0 real fault

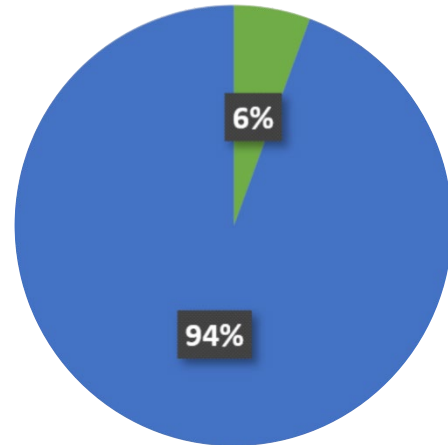


Figure 86: class 1 real fault

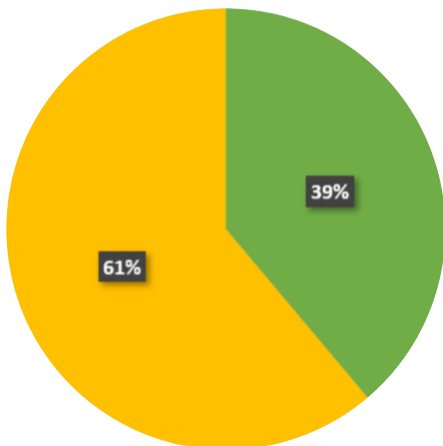


Figure 84: class 5 real fault

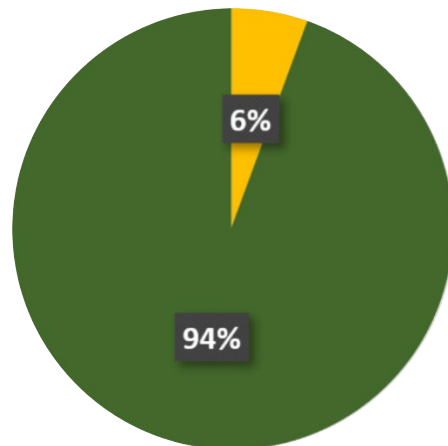


Figure 85: class 6 real fault

Class number	Damage type
0	No damage (healthy pump)
1	Extremely damaged valve plate
5	Slipper damage
6	Cylinder damage

Table 7: damage class legend

## 8.3 Test 3: Multiple Faults

In this chapter, different fault combinations will be taken into account. In particular, 8 different classes will be considered:

- 0: Healthy pump
- 1: extremely damaged valve plate
- 2: extremely damaged valve plate + cylinder leakage
- 3: extremely damaged valve plate + cylinder leakage + slipper damage
- 4: extremely damaged valve plate + slipper damage
- 5: slipper damage
- 6: cylinder leakage
- 7: slipper + cylinder damage

As sensor, will be considered pressure ripple, outlet pressure, speed, drain pressure.

This test has given low accuracy results: the best value obtained is 54%, using quadratic SVM.

In particular, the most difficult combination is extremely damaged valve plate and slipper fault.

As shown in previous test, leakage fault seems to be the biggest source of bias. Probably, a more precise model for this loss is required.

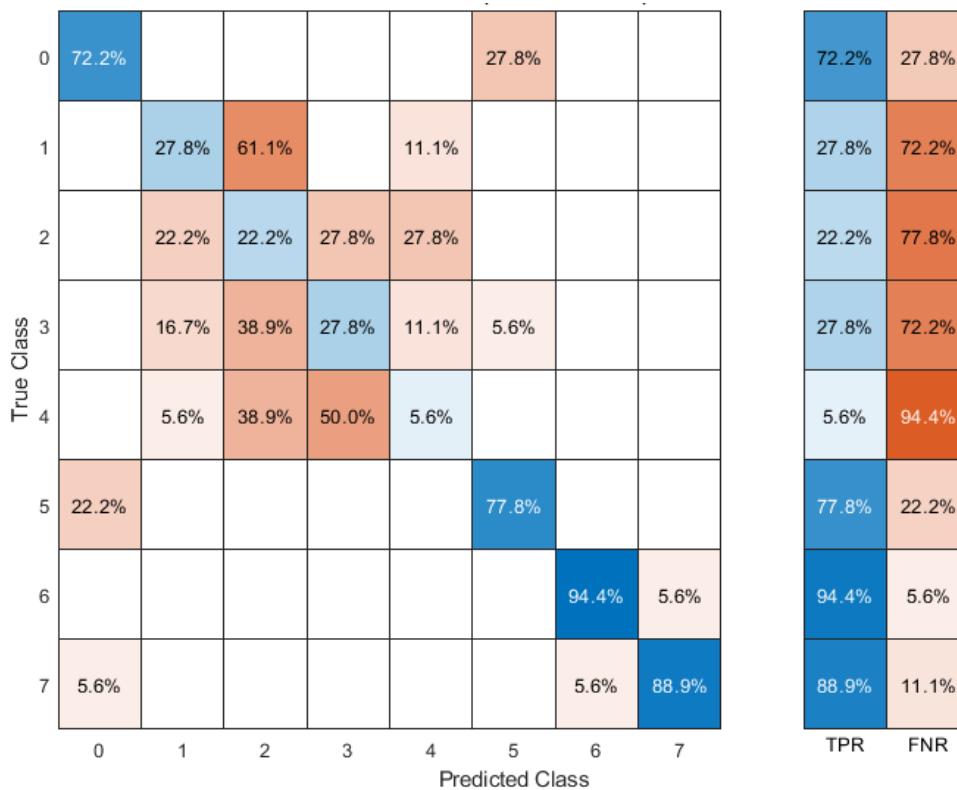


Figure 88: confusion matrix test 3

The pie charts in figures 85,86,87,88,89,90,91,92 shows the accuracy of the model for each single class.

Table iii shows the classes legend.

- Healthy    ■ ED valveplate    ■ ED + cyl fault    ■ ED + cyl leak + slipper fault
- ED + Slipper fault    ■ Slipper fault    ■ Cyl fault    ■ Slipper fault + cyl fault

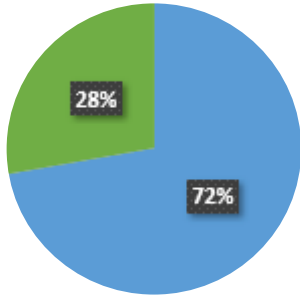


Figure 91: class 0 real fault

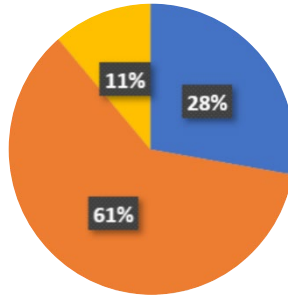


Figure 90: class 1 real fault

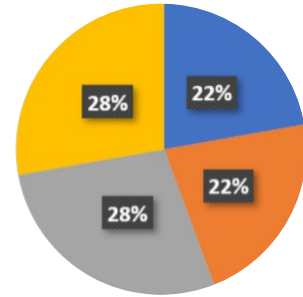


Figure 89: class 2 real fault

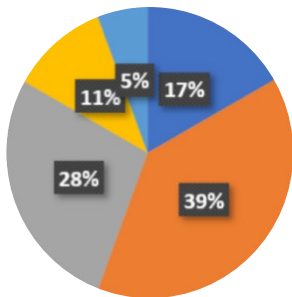


Figure 94: class 3 real fault

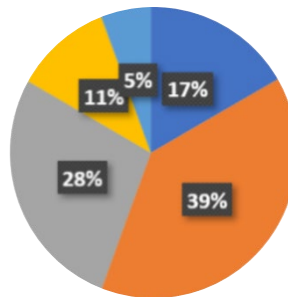


Figure 93: class 4 real fault

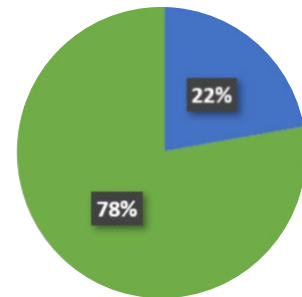


Figure 92: class 5 real fault

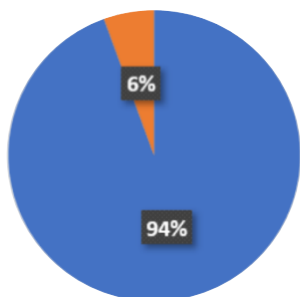


Figure 96: class 6 real fault

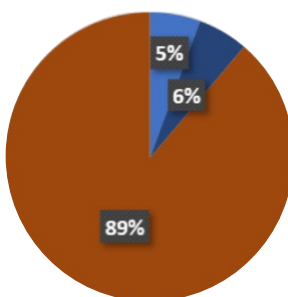


Figure 95: class 7 real fault

Condition number	description
0	Healthy pump
1	Extremely damaged valve plate
2	ED valveplate + cyl fault
3	ED valveplate + cyl fault + slipper fault
4	ED valveplate + slipper fault
5	Slipper fault
6	Cylinder fault
7	Slipper fault + cylinder fault

*Table 8: condition number legend (fault combination)*

# 9 CONCLUSIONS AND FUTURE WORK

During this research work, different issues have been faced both from experimental point of view, and from simulation one.

Lumped parameter model can be considered validate in steady state conditions.

The proposed approach had made possible to create different faults without damaging the internal component of the pump.

Finally, the condition monitoring model has shown a good accuracy (85%) to detect different faults separately.

The combination of faults has been difficult to detect, probably because of the model limits.

In future research, a more precise model could be used instead of a lumped parameter one. It will be crucial find a good compromise between model complexity and condition monitoring algorithm accuracy.

# Appendix 1: AVAS tool

To get the opening area plot, AVAS tool (Automated Valve plate Area Search) has been used. This program, developed by Shanmukh Sarode and Swarnava Mukherjee is able to get the minimum area normal to the streamline for every shaft position. The fluid volume used to compute the minimum area is shown in figure 93. The AVAS working flow is depicted in figure 94

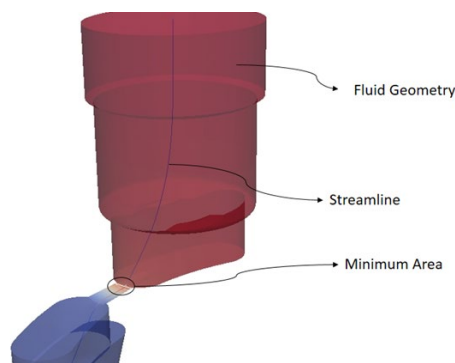


Figure 97: example of fluid volume used for minimum area computation

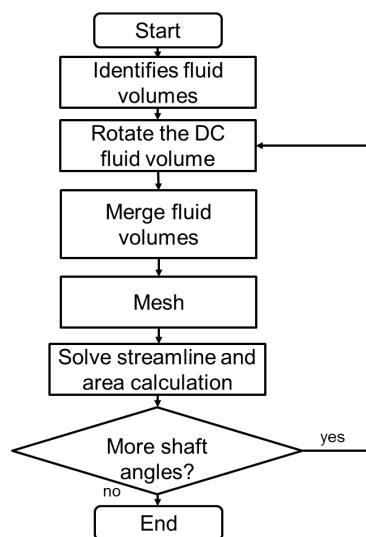


Figure 98: AVAS tool workflow

As final output, the tool is able to provide the plot shown in figure 95.

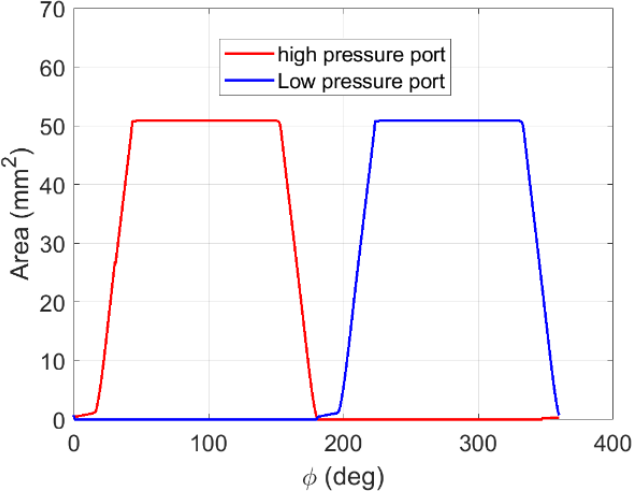


Figure 99: example of area file

# Appendix 2: DAQ calibration

To calibrate pressure sensors data acquisition system, different pressure values have been sent using a hand pump in picture 96, taken from Keller catalog to the sensors and the correspondent sensor output voltage have been measured.



Figure 100: example of hand pump used to test pressure sensors

An example of pressure vs voltage plot is shown in figure 97. The trendline equation gives the relation between pressure and voltage.

Table iii resume calibration factor (trendline slope and trendline offset) necessary to convert the read voltage in pressure value.

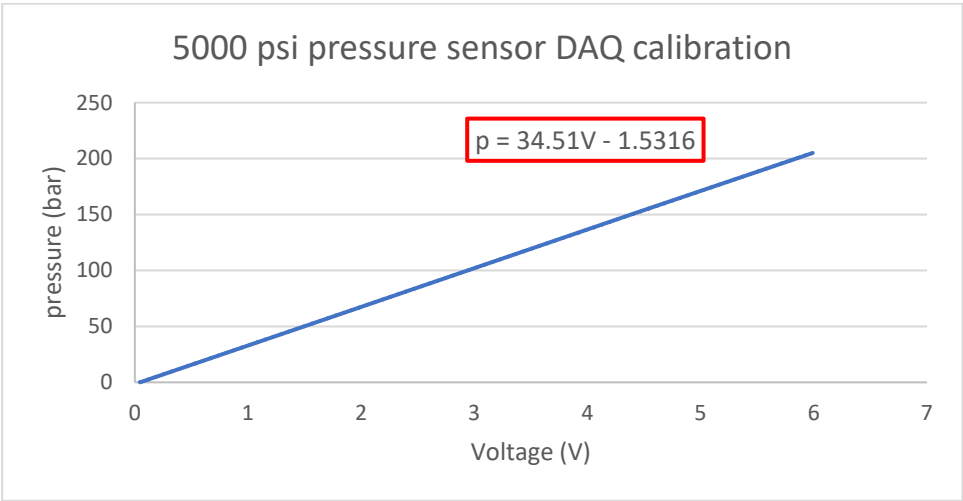


Figure 101: pressure vs voltage plot

Full scale	slope	offset
6000 psi	41.446	-0.3569
5000 psi	34.51	-1.5316
250 bar	25.012	-2.3681

Table 9: pressure sensor conversion factors

# Appendix 3: Fft And Nyquist's Theorem

Fast fourier transform, or fft, refers to an algorithm able to compute the discrete Fourier transform (DFT) in a faster way.

The DFT can be expressed by the equation 31.

$$x[k] = \sum_{n=0}^{N-1} x_n e^{\frac{-j2\pi kn}{N}} \quad (31)$$

Where N is the size of the domain.

This procedure is very time and computationally expensive, because it requires to sum and multiply a large amount of data.

Coley and Turkey [23] showed that the DFT can be divided into 2 sub-parts (eq. 32 and 33)

$$x[k] = \sum_{m=0}^{N/2-1} x_{2m} \cdot e^{\frac{-j2\pi k(2m)}{N}} + \sum_{m=0}^{N/2-1} x_{2m+1} \cdot e^{\frac{-j2\pi k(2m+1)}{N}} \quad (32)$$

$$x[k] = \sum_{m=0}^{N/2-1} x_{2m} \cdot e^{\frac{-j2\pi k(m)}{(N/2)}} + e^{\frac{-j2\pi k}{N}} \sum_{m=0}^{N/2-1} x_{2m+1} \cdot e^{\frac{-j2\pi k(m)}{(N/2)}} \quad (33)$$

Those 2 terms are computed from zero to N/2 +1, that means that the computational time will be halved.

It is possible to apply this method in a recursive way, decreasing again the computational effort.

The threshold is reached when further divisions are not advantageous anymore.

FFT operator is applied to the signal in time domain to get a value in frequency domain. During the data acquisition part, it is crucial to avoid aliasing. This phenomenon occurs when the acquisition system is not able to correctly transfer the information from analog domain to digital one.

An example of aliasing is shown in figure 98 [23]. It is possible to see that in case of undersampling the sinusoid can be read as one with different frequency with respect to the original one.

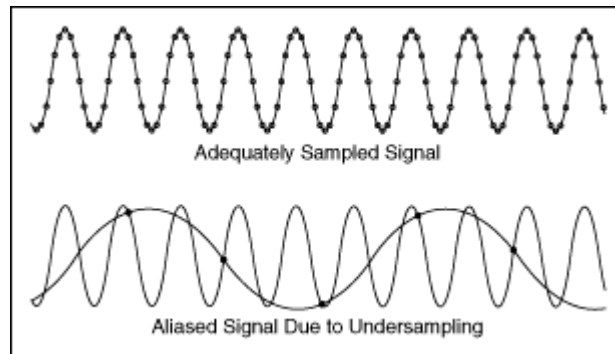


Figure 102: example of aliasing effect

When aliasing occurs, it is not possible to truly know the signal shape.

The Shannon's theorem states that a continuous-time signal  $x(t)$  with frequencies no higher than the maximum signal frequency  $f_{max}$  can be reconstructed exactly from its samples  $x[n] = x(nT_s)$ , if the samples are taken a rate  $f_s = 1 / T_s$  that is greater than  $2 f_{max}$ .

The minimum sampling rate, that is  $f_{max}$ , is called Nyquist rate.

# 10 Bibliography

- [1] R. K. Mobley, *An Introduction to predictive Maintenance*. 2007.
- [2] Parker, "8 Reasons You Can't Afford to Ignore Condition Monitoring," 2016.
- [3] J. Kane, T. D. Richmond, and D. N. Robb, "Paper 3: Noise in Hydrostatic Systems and its Suppression," *Proceedings of the Institution of Mechanical Engineers, Conference Proceedings*, vol. 180, no. 12, pp. 36–52, Jun. 1965, doi: 10.1243/pime\_conf\_1965\_180\_348\_02.
- [4] B. O. Helgestad, K. Foster, and F. K. Bannister, "Pressure transients in an axial piston hydraulic pump.," *INST. MECH. ENGR. PROC.*, vol. 88, no. 1977, pp. 189–199.
- [5] W. ZHOU, S. LU, G. WU, and J. ZHOU, "Research on condition monitoring failure in axial piston pumps," *Proceedings of the JFPS International Symposium on Fluid Power*, 1993, doi: 10.5739/isfp.1993.229.
- [6] Y. GAO, X. KONG, and Q. ZHANG, "WAVELET APPROACH FOR PERFORMANCE MONITORING AND DIAGNOSIS OF A HYDRAULIC PUMP," *Proceedings of the JFPS International Symposium on Fluid Power*, 2005, doi: 10.5739/isfp.2005.711.
- [7] P. Casoli, M. Pastori, F. Scolari, and M. Rundo, "A vibration signal-based method for fault identification and classification in hydraulic axial piston pumps," *Energies*, 2019, doi: 10.3390/en12050953.
- [8] T. T. Le, J. Watton, and D. T. Pham, "An artificial neural network based approach to fault diagnosis and classification of fluid power systems," *Proceedings of the Institution of Mechanical Engineers. Part I: Journal of Systems and Control Engineering*, 1997, doi: 10.1243/0959651971539830.
- [9] T. Kivelä and J. Mattila, "Internal leakage fault detection for variable displacement axial piston pump," 2013. doi: 10.1115/FPMC2013-4445.
- [10] J. Yan, H. Zhu, X. Yang, Y. Cao, and L. Shao, "2259. Research on fault diagnosis of hydraulic pump using convolutional neural network," *Journal of Vibroengineering*, 2016, doi: 10.21595/jve.2016.16956.
- [11] S. Saha, "A Comprehensive Guide to Convolutional Neural Networks — the ELI5 way," 2018.
- [12] Y. Lan *et al.*, "Fault diagnosis on slipper abrasion of axial piston pump based on Extreme Learning Machine," *Measurement: Journal of the International Measurement Confederation*, 2018, doi: 10.1016/j.measurement.2018.03.050.
- [13] K. Erdem, "Introduction to Extreme Learning Machines," 2020.
- [14] K. Erdem, "Introduction to Extreme Learning Machines," 2020.
- [15] M. Ivantysynova, "Hydrostatic Pumps and Motors.pdf."
- [16] N. Keller, "CONDITION MONITORING SYSTEMS FOR AXIAL PISTON PUMPS: MOBILE APPLICATIONS," 2020.
- [17] A. Corvaglia and M. Rundo, "Comparison of 0D and 3D Hydraulic Models for Axial Piston Pumps," 2018.
- [18] M. Pelosi, "AN INVESTIGATION ON THE FLUID-STRUCTURE INTERACTION OF PISTON/CYLINDER INTERFACE," 2012.
- [19] Danfoss, "Failure Analysis and Parts Evaluation," 2014.
- [20] I. Goodfellow, Y. Bengio, and A. Courville, *Deep Learning*. 2016.
- [21] baeldung, "Multiclass Classification Using Support Vector Machines," 2020.
- [22] R. de Wet, "Manhattan Distance Calculator," 2021.

- [23] J. W. Cooley and J. W. Turkey, "An algorithm for the machine calculation of complex Fourier series.," 1965.